Acetylcholine receptors in the retinas of the α7 nicotinic acetylcholine receptor knockout mouse

Marci L. Smith,[1] Fred G. Oliveira Souza,[1] Kady S. Bruce,[1] Christianne E. Strang,[1] Barbara J. Morley,[2] Kent T. Keyser[1]

[1]*Department of Vision Sciences, University of Alabama at Birmingham, Birmingham, AL;* [2]*Boys Town National Research Hospital, Omaha, NE*

Purpose: The α7 nicotinic acetylcholine receptor (nAChR) is widely expressed in the nervous system, including in the inner retinal neurons in all species studied to date. Although reductions in the expression of α7 nAChRs are thought to contribute to the memory and visual deficits reported in Alzheimer's disease (AD) and schizophrenia , the α7 nAChR knockout (KO) mouse is viable and has only slight visual dysfunction. The absence of a major phenotypic abnormality may be attributable to developmental mechanisms that serve to compensate for α7 nAChR loss. We hypothesized that the upregulation of genes encoding other nAChR subunits or muscarinic acetylcholine receptor (mAChR) subtypes during development partially accounts for the absence of major deficiencies in the α7 nAChR KO mouse. The purpose of this study was to determine whether the deletion of the α7 nAChR subunit in a mouse model resulted in changes in the regulation of other cholinergic receptors or other ion channels in an α7 nAChR KO mouse when compared to a wild-type (WT) mouse.

Methods: To examine gene expression changes, we employed a quantitative real-time polymerase chain reaction (qPCR) using whole retina RNA extracts as well as RNA extracted from selected regions of the retina. These extracts were collected using laser capture microdissection (LCM). The presence of acetylcholine receptor (AChR) subunit and subtype proteins was determined via western blotting. To determine any differences in the number and distribution of choline acetyltransferase (ChAT) amacrine cells, we employed wholemount and vertical immunohistochemistry (IHC) and cell counting. Additionally, in both WT and α7 nAChR KO mouse retinas, the distribution of the nAChR subunit and mAChR subtype proteins were determined via IHC for those KO mice that experienced mRNA changes.

Results: In the whole retina, there was a statistically significant upregulation of α2, α9, α10, β4, nAChR subunit, and m1 and m4 mAChR subtype transcripts in the α7 nAChR KO mice. However, the retinal layers showed complex patterns of transcript expression. In the ganglion cell layer (GCL), m2 and m4 mAChR subtype transcripts were significantly upregulated, while β3 and β4 nAChR subunit transcripts were significantly downregulated. In the inner portion of the inner nuclear layer (iINL), α2, α9, β4, nAChR subunit, and m3 and m4 mAChR subtype transcripts were significantly downregulated. In the outer portion of the inner nuclear layer (oINL), β2, β4, and m4 AChR subunit transcripts were significantly upregulated. Western blot experiments confirmed the protein expression of α3−α5 and α9-containing nAChR subunits and m1−m2 mAChR subtypes in mouse retinas. IHC results supported many of the mRNA changes observed. Finally, this is the first report of α9 and α10 nAChR subunit expressions in the retina of any species.

Conclusions: Rather than a simple upregulation of a single AChR subunit or subtype, the absence of the α7 nAChR in the KO mice was associated with complex layer-specific changes in the expression of AChR subunits and subtypes.

While the major excitatory neurotransmitter in the retina is glutamate, the other excitatory neurotransmitter expressed in the retina is acetylcholine (ACh). ACh is synthesized from choline and Acetyl Co-A by the enzyme choline acetyltransferase (ChAT). There are two sources of ACh in the retina: the populations of starburst amacrine cells and displaced starburst amacrine cells. Starburst amacrine cells have cell bodies in the inner nuclear layer (INL) that project to the OFF sublamina of the inner plexiform layer (IPL) and release ACh in response to light decrements [1,2]. Displaced starburst amacrine cells have cell bodies in the ganglion cell layer (GCL) that project to the ON sublamina of the IPL and release ACh in response to light increments [2,3]. Additionally, there is a light-independent tonic release of ACh in the retina [2]. Both populations release gamma-aminobutyric acid (GABA) and ACh, and both receive glutamatergic inputs from cone bipolar cells mediated by kainate receptors [2].

Acetylcholine receptors (AChRs) are expressed by photoreceptor, bipolar, amacrine, displaced amacrine, horizontal, and ganglion cells [4-9]. AChR activation has been shown to affect ganglion cell light responses and has been shown to play a role in retinal development [10-12].

There are two classes of AChRs: muscarinic (mAChRs and nicotinic (nAChRs. The mAChRs are G-protein coupled

Correspondence to: Marci Smith, Department of Vision Science, University of Alabama at Birmingham, Birmingham, AL; Phone: (205) 975-0577; FAX: (205) 934-3425; email: mercury1@uab.edu

receptors of which there are five subtypes, m1–m5, each encoded by a specific gene. In general, mAChRs are activated by acetylcholine, choline, and muscarine, and they are blocked by atropine [13]. The mAChRs fall into two general categories: those where activation generally results in excitation or those where activation generally results in inhibition [14]. The m1, m3, and m5 subtypes all activate the phosphatidyl inositol or phospholipase signaling pathways via activation of the Gq-α G-protein. Activation of these receptor subtypes causes the release of intracellular Ca^{2+}, the inhibition of Ca^{2+}-activated K^+ channels, and the activation of nonspecific cation channels, which lead to cell depolarization [13]. The m2 and m4 subtypes inhibit adenylate cyclase and cyclic adenosine monophosphate production via activation of the Gi-α G-protein. Activation of these subtypes causes inhibition of the Ca^{2+} channels and activation of the K^+ channels, which leads to cell hyperpolarization [15].

The nAChRs are pentameric, mixed-cation channels that are members of the ligand-gated ion channel superfamily [16,17]. Depending on the subtype, nAChRs have 2–5 agonist binding sites. In general, nAChRs are activated by ACh, carbachol, and nicotine, and they are blocked by curare. The nAChRs, typically expressed in neurons, are composed of α2−α7 and β2−4 subunits. The subunit expressions of α9 and α10 have been found in neuroepithelial and immune cells [18-20]. As well, nAChR subunits can combine to form a large number of receptors with specific pharmacological and physiologic profiles [21-23]. For example, the α2−α6 and the β2−β4 subunits form heteromeric receptors that are insensitive to α-bungarotoxin (α-BGT) and desensitize more slowly [21-27]. In addition, α7 subunits form homomeric nAChRs that are sensitive to α-BGT and desensitize rapidly, and α7 nAChR subunits can form heteromeric receptors with β2 nAChR subunits [27]. Unlike the other nAChRs, α9-containing nAChRs are activated by ACh, but they are blocked by nicotine, α-BGT strychnine, and atropine. Furthermore, α9 may form a homomeric receptor in vitro, but it is thought to form a heteromeric α9α10 nAChR in vivo [28-36], while α9/10 heteromeric nAChRs demonstrate a pharmacology similar to that of α9 homomeric nAChRs, but with faster desensitization [37]. Compared to the other nAChR subtypes, the α7, α9, α9/10, α3β2α5, and α3β4α5 nAChRs all have high Ca^{2+} permeability [36,38,39].

In some animal models, including the rabbit, the α7 nAChR subtype is widely expressed throughout the inner retina and has been shown to affect ganglion cell responses directly and indirectly [5,40,41]. First, subpopulations of ganglion cells express α7 nAChRs, and the activation of these receptors can directly affect the responses of these ganglion cells [41]. Second, subsets of amacrine cells containing glycine, or GABA, express α7 nAChRs [5,40]. The activation of α7 nAChRs leads to the depolarization of amacrine cells, increasing the release of inhibitory neurotransmitters from amacrine cells and providing an indirect cholinergic inhibition of the ganglion cell responses. Additionally, subpopulations of ON cone bipolar cells express α7 nAChRs [5].

A reduction in the α7 nAChR expression has been observed in patients with Alzheimer's disease (AD) and schizophrenia, both of which are characterized by visual dysfunctions attributable to changes at the level of the retina and in the visual cortex [42-45]. Because of the link between these diseases and α7 nAChRs, one would predict visual system deficits in the α7 nAChR KO mice. However, α7 nAChR KO mice have only slightly reduced visual acuity [46-52]. Additionally, the reduction in visual acuity in these mice has been linked to changes in the cortex, and retinal changes have not been reported [47]. Thus, we predicted that the upregulation of other AChRs, particularly those with high Ca^{2+} permeability or those that increase intracellular $[Ca^{2+}]$, may partially compensate for the loss of α7 nAChRs. To test this prediction, we first determined whether there were changes in the mRNA expressions of nAChR subunit transcripts and mAChR subtype transcripts in the whole retina. Second, we investigated whether there were retinal cell, layer-specific changes in the expressions of AChR subunit and subtype transcripts. We then determined whether compensation for the loss of the α7 nAChR subunit was correlated with the changes in the number of cholinergic cells. Finally, we confirmed the presence of AChR subunit and subtype proteins, and we visualized the distribution of a subset of AChR subunits and subtypes that had changes in mRNA expression levels via western blotting and immunohistochemistry (IHC).

METHODS

Animals and tissue: Retinas, eyecups, and brains from wild-type (WT) and the α7 nAChR, α9, and α10 KO mice were provided by Dr. Barbara Morley at Boys Town National Research Hospital (BTNRH; Omaha, NE). Heterozygote breeders for the α7 knockout (KO) mouse strain on the C57Bl/6J (B6) background were purchased from the Jackson Laboratory (Bar Harbor, ME, USA), and a colony was established at BTNRH. The α7 KO mouse model was initially developed and characterized by Orr-Urteger et al. (1997) and Paylor et al. (1998). The nAChR α9 and α10 KO mouse models were generated by the deletion of exons 1 and 2, which contained the translation/transcription initiation sites, and they were confirmed by Southern blotting (Genoway,

Inc., Lyon Cedex, France). The KO lines were subsequently backcrossed at BTNRH to B6 mice using marker-assisted accelerated backcrossing (Max Bax; Charles River, Wilmington, MA) until congenicity was achieved. The absence of α9 or α10 subunit transcripts was verified by polymerase chain reaction (PCR) and quantitative real-time polymerase chain reaction (qPCR), while employing a custom PCR array (Qiagen, Frederick, MD) using samples from WT mouse cochlear tissue as the positive control, as α9 and α10 KO mice have the expected cochlear phenotype of aberrant innervation of the hair cells. Care and animal-use procedures were in strict accordance with the National Institutes of Health Guide for the Care and Use of Animals and were approved by the BTNRH IACUC. Retinas to be used in qPCR experiments were obtained by enucleation and hemisection, followed by dissection from the sclera and the choroid. Once retinas were isolated, they were flash frozen, shipped on dry ice, and stored at −80 °C before RNA extraction. Retinas from 11 α7 nAChR KO, 2 α9 nAChR KO, 2 α10 nAChR KO, and an equal number of WT littermates were used in whole retina qPCR experiments. Retinas from the same animals were pooled before RNA extraction. Eyecups to be used for laser capture microdissection (LCM) were embedded in a block of optimal cutting temperature medium immediately following enucleation (Sakura Finetek, Torrance, CA). Then, they were frozen, sectioned into 8 µm vertical cryosections (Leica CM 3050), mounted onto polyethylene napthalate membrane glass slides (Applied Biosystems, Foster City, CA), and stored at −80 °C. Retinas from 11 α7 nAChR KO and 11 WT mice were used for LCM. Samples collected from the same retinal layers in the same animals, both the right and left eyes, were pooled. Brains were collected from the C57BL/6J WT mice and were flash frozen immediately following removal, shipped on dry ice, and stored at −20 °C until RNA extraction. RNA extracted from mouse brain was used in custom primer optimization experiments. Retinas to be used for western blotting were obtained by enucleation and hemisection, followed by dissection from the sclera and the choroid. Once retinas were isolated, they were flash frozen, shipped on dry ice, and stored at −80 °C before protein extraction. Eyecups to be used for IHC were obtained by enucleation followed by hemisection. Eyecups were then fixed in 1% paraformaldehyde with 0.34% L-lysine and 0.05% sodium-m-periodate in 0.1 M PBS (1% PLP) for 2 h at room temperature. They were then cryoprotected by immersion in graded concentrations of sucrose (10%, 20%, and then 30%) in 0.1 M PBS and then stored at 4 °C. Retinas from five α7 nAChR KO and five WT mice were used for wholemount IHC experiments, and a different set of five retinas from α7 nAChR KO and five

retinas from WT mice were used for vertical IHC double label experiments.

RNA extraction protocol: For qPCR studies, total RNA was extracted from flash-frozen retinas using the RNAqueous −4PCR kit (Ambion; Austin, TX). The extractions yielded an RNA concentration of 60–100 ng/ul for each retina. The quality of the RNA was assessed using ratios of 260/280 nm and 260/230 nm, as measured by the Nanodrop ND-1000 spectrophotometer (Thermo Scientific; Wilmington, DE). The PicoPure RNA isolation kit (Arcturus; Sunnyvale, CA) was used to extract RNA from specific retinal layers that were isolated via LCM (as described below). This protocol followed steps equivalent to the RNAqueous kit, but it was optimized for samples as small as one cell.

qPCR array screening: Custom 96-well PCR arrays (SABiosciences; Frederick, MD) containing pre-optimized and pre-validated primers were used to determine whether the α7 nAChR KO mice experienced changes in the mRNA expressions of 96 receptors, channels, or transporters, including AChRs. The arrays used in this study contained primers to a wide variety of neuronal receptors, channels, and transporters, including GABA receptors, glycine receptors, and potassium channels (Table 1). The arrays also contained a positive PCR control, a reaction lacking reverse transcriptase, a mouse DNA positive control, and several reference genes, including including β-actin (*ACTB*) and glyceraldehyde-3-phosphate dehydrogenase (*GAPDH*). SuperArray plates enabled the screening of many targets, but their primer sets were proprietary. Thus, sequencing of the products could not be completed as we could not obtain primer sequences.

RNA was extracted from eight KO and eight WT mice and quality assessed following the same protocol previously described. The RNA was converted to cDNA using an RT² First Strand kit (SABiosciences; Frederick, MD).

Quantification: For qPCR experiments in this study, the threshold was set at 90 relative fluorescent units (RFU). The cycle at which a sample's amplification curve crosses the threshold line is the cycle threshold (Ct). Fold change (up- or downregulation) was determined using the ΔΔ Ct method. A standard independent sample, two-tailed *t* test was performed to determine whether there was a significant difference in the KO and WT samples for each target gene. The total standard deviation (SD) was calculated by first determining the SD of both the WT and KO samples. The SD for each sample was calculated by subtracting the square root of the average of the squared differences from the mean. Then, the sample SDs were used to calculate the total SD for the fold change by taking the square root of the squared SD for the WT samples plus the squared SD for the KO samples. The standard error
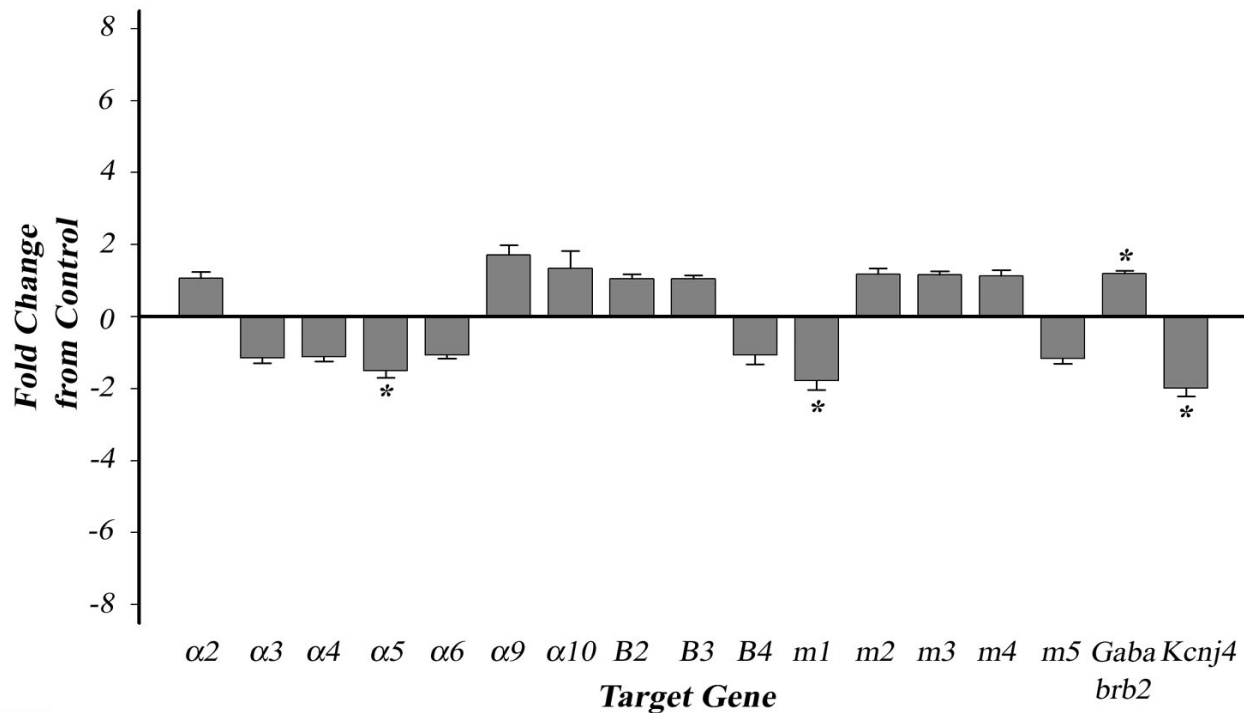
Figure 1. SuperArray quantitative real-time polymerase chain reaction (qPCR) screening of fold changes in mouse retina. The qPCR showed a significant upregulation of the β2 GABA$_A$ receptor subunit and a downregulation of the α5 nicotinic acetylcholine receptor (nAChR) subunit, the m1 muscarinic acetylcholine receptor (mAChR) subtype, and the Kcnj4 channel. Error bars represent the standard error of mean (SEM). *p<0.05.

of the mean (SEM) was calculated by dividing the total SD by the square root of the sample size.

AChR qPCR primer design and optimization: To confirm any changes in expressions relative to those identified in qPCR arrays and screenings, as well as to perform a more fine-grained analysis of changes in the nAChR subunit and mAChR subtype expressions in the α7 nAChR KO mouse retinas, primers were designed for nAChR subunits and mAChR subtypes using a Beacon Designer (Table 1). The Ryanodine receptor 3 (*RyR3*) was chosen as the reference gene because the results of our qPCR screening experiments showed that its expression did not differ between WT and α7 nAChR KO mouse samples (Table 2). All primer sets were purchased from Sigma-Genosis (St. Louis, MO). Primers were previously used to determine the presence of AChRs in the mouse retinas (RT–PCR), but further optimization steps were performed to ensure primers were appropriate for qPCR [53].

Optimization for qPCR included determining the annealing temperature and primer concentration ratio that resulted in the highest copy number and a single product

for each primer set. RNA for optimization experiments was extracted from the whole brain tissue of WT mice using the RNAqueous −4PCR kit, as previously described. RNA was converted to cDNA using an iScript cDNA synthesis kit (BioRad; Hercules, CA). One microgram of RNA was added to a cDNA synthesis mix containing 5×iScript buffer, iScript reverse transcriptase (includes an RNase inhibitor), and RNase-free water. The cDNA synthesis mix was placed in the MyCycler Personal Thermocycler (BioRad; Hercules, CA) and incubated at 25 °C for 5 min, at 45 °C for 30 min, and at 85 °C for 5 min. For amplification, 200 nanograms of cDNA were added to a PCR mix containing iQ SYBR green supermix (containing DNA polymerase and dNTPs; BioRad, Hercules, CA), nuclease-free water, and forward and reverse primers. The cDNA/PCR mix was placed in the thermocycler (BioRad iQ5) and underwent an initial hot start at 95 °C for 3 min followed by 40 cycles at 95 °C for 10 s (denaturation), at an optimum annealing temperature for 30 s, and at 72 °C for 30 s (elongation). A melt curve to determine the melting point of the DNA product was performed immediately after the

TABLE 1. SUPERARRAY qPCR SCREENING TARGETS AND FOLD CHANGE BETWEEN WT AND α7 NAChR KO MICE.

Target	Description	Fold change
Accn1	amiloride-sensitive cation channel 1, neuronal, hair cell	−1.03
Accn2	neuronal asic 1a	−1.17
Accn3	amiloride-sensitive cation channel 3, dorsal root ganglion	1.06
Cacna1a	calcium channel, voltage-dependent, P/Q type, α 1A, brain	1.17
Cacna1b	calcium channel, voltage-dependent, N type, α 1B, brain sensory	1.00
Cacna1g	calcium channel, voltage-dependent, T type cardiac and brain	−1.03
Cacna1h	calcium channel, voltage-dependent, T type, α 1H, neuronal	−1.08
Cacnb3	calcium channel, voltage-dependent, β 3 subunit, olfactory bulb	−1.03
Cacnb4	voltage gated calcium channel lymphocytes, cardiac and absence seizures	−1.07
Cftr	CFTR	1.15
Chat	choline acetyltransferase (Chat)	1.09
Chrm1	cholinergic receptor, muscarinic 1 brain	**-1.78***
Chrm2	cholinergic receptor, muscarinic 2, cardiac	1.18
Chrm3	cholinergic receptor, muscarinic 3, cardiac	1.17
Chrm4	cholinergic receptor, muscarinic 4 brain	1.12
Chrm5	cholinergic receptor, muscarinic 5 brain	−1.16
Chrna1	cholinergic receptor, nicotinic, α polypeptide 1	−1.08
Chrna2	cholinergic receptor, nicotinic, α polypeptide 2	1.06
Chrna3	cholinergic receptor, nicotinic, α polypeptide 3	−1.15
Chrna4	cholinergic receptor, nicotinic, α polypeptide 4, brain	−1.12
Chrna5	cholinergic receptor, nicotinic, α polypeptide 5	**-1.50***
Chrna6	cholinergic receptor, nicotinic, α polypeptide 6	−1.07
Chrna7	cholinergic receptor, nicotinic, α polypeptide 7	**-103.61***
Chrna9	cholinergic receptor, nicotinic, α polypeptide 9	1.72
Chrna10	cholinergic receptor, nicotinic, α polypeptide 10	1.33
Chrnb1	cholinergic receptor, nicotinic, β polypeptide 1, motor neurons	1.18
Chrnb2	cholinergic receptor, nicotinic, β polypeptide 2	1.00
Chrnb4	cholinergic receptor, nicotinic, β polypeptide 4	−1.06
Htr3a	5HT 3a	−1.13
Chrnb3	cholinergic receptor, nicotinic, β polypeptide 3	1.05
Clca1	chloride channel calcium activated 1 (Clca1), brain	−1.03
Clcn2	chloride channel 2, astrocytes, salivary gland	1.20
Clcn4−2	chloride channel 4−2 (Clcn4−2), taste bud, brain	1.15

Target	Description	Fold change
Clcn6	chloride channel 6, brain	−1.07
Gabra1	λ-aminobutyric acid (GABA-A) receptor, subunit α 1	1.02
Gabra2	λ-aminobutyric acid (GABA-A) receptor, subunit α 2	−1.10
Gabra3	λ-aminobutyric acid (GABA-A) receptor, subunit α 3	−1.07
Gabra4	λ-aminobutyric acid (GABA-A) receptor, subunit α 4	1.15
Gabra5	λ-aminobutyric acid (GABA-A) receptor, subunit α 5	1.08
Gabra6	λ-aminobutyric acid (GABA-A) receptor, subunit α 6	NA
Gabrb2	λ-aminobutyric acid (GABA-A) receptor, subunit β 2	**1.19***
Gabrb3	λ-aminobutyric acid (GABA-A) receptor, subunit β 3	1.07
Gabrd	λ-aminobutyric acid (GABA-A) receptor, subunit Δ	1.03
Gabrg2	λ-aminobutyric acid (GABA-A) receptor, subunit λ 2	1.16
Gabrp	λ-aminobutyric acid (GABA-A) receptor, π	−1.36
Gabrq	λ-aminobutyric acid (GABA-A) receptor, subunit θ	−1.04
Gabrr1	λ-aminobutyric acid (GABA-C) receptor, subunit ρ 1	−1.09
Gabrr2	λ-aminobutyric acid (GABA-A) receptor, subunit ρ 2	1.10
Gabrr3	λ-aminobutyric acid (GABA-A) receptor, subunit ρ 3	1.07
Glra1	glycine receptor α 1	1.09
Glra2	glycine receptor, α 2 subunit	1.15
Glra3	glycine receptor, α 3 subunit	−1.20
Glra4	glycine receptor, α 4	1.01
Glrb	glycine receptor, β subunit	−1.06
Kcna2	potassium voltage-gated channel, shaker-related, brain and spinal cord	1.02
Kcna6	potassium voltage-gated channel, shaker-related, brain	−1.04
Kcnc4	potassium voltage gated channel, Shaw-related, neurotransmitter release	1.06
Kcnd1	potassium voltage-gated channel, Shal, brain	−1.01
Kcnh2	potassium voltage-gated channel, subfamily H, brain, ear	−1.03
Kcnj3	potassium inwardly-rectifying channel, subfamily J, spinal interneurons	−1.09
Kcnj4	frontal cortex pyramidal neurons HCN, Kir2, and Kleak	**−1.98***
Kcnj6	potassium inwardly-rectifying channel, subfamily J, brain	1.01
Kcnn2	potassium channel calcium-activated, subfamily N, synaptic plasticity	1.21
Kcnn3	potassium intermediate/small conductance, Ca²⁺ activated, N type, brain	−1.28
Kcnq2	potassium voltage-gated channel, subfamily Q, hippocampus	1.02
Kcnq3	potassium voltage-gated channel, subfamily Q, member 3, brain	1.18
Ryr3	ryanodine receptor 3	1.22

Target	Description	Fold change
Scn1a	sodium channel, voltage-gated, type I, brain	1.08
Scn1b	sodium channel, voltage-gated, type I, β brain & cardiac	−1.12
Scn5a	sodium channel, voltage-gated, type V, cardiac and brain	1.29
Scn7a	sodium channel, voltage-gated, type VII, sodium concentration sensor, taste	1.07
Slc5a7	solute carrier family 5 (high affinity choline transporter), member 7	−1.01
Gria1	AMPA 1 cerebllum	1.03
Gria2	AMPA 2 synaptic	1.14
Gria3	AMPA 3, als	1.14
Gria4	AMPA 4 alcohol use	1.19
Grik1	kainate 1 presynaptic	1.06
Grik2	kainate 2 mossy fiber, synaptic plasticity	1.11
Grik5	kainate 5 mossy fiber	1.15
Grin1	NMDA NR1 brain	−1.05
Grin2a	NMDA NR2a brain	−1.08
Grin2b	NMDA NR2b brain	1.17
Grin2c	NMDA NR2c brain	1.13
Grin2d	NMDA NR2d brain	−1.16
Grin3a	NMDA NR3a	1.04
Grin3b	NMDA3b motor neurons	1.09
Vdac1	voltage-dependent anion channel 1	1.02
Hsp90ab1	heat shock protein 90 α (cytosolic), class B member 1	1.16
Actb	actin, β	Avg Ct=22.3
Gapdh	glyceraldehyde-3-phosphate dehydrogenase	Avg Ct=23.4
Gusb	glucuronidase, β	Avg Ct=32.6
Hprt1	hypoxanthine guanine phosphoribosyl transferase 1	Avg Ct=23.8
MGDC	mouse genomic DNA contamination	No amp
RTC	reverse transcription control	No amp
PPC	positive PCR control	Avg Ct=18

* $p < 0.05$ *** $p < 0.001$

TABLE 2. ACETYLCHOLINE RECEPTOR PRIMER PAIRS.

Subunit	Accession number	Primer (5'-3')	Product (bp)	Temp (C°)	Primer ratio (nmol)	Product homology to mouse sequence
α2 nAChR	NM_144803	F- GTGCCCAACACTTCCGATG R-TGTAGTCATTCCATTCCTGCTTT	126	55.8	F400:R600	92%
α3 nAChR	NM_145129	F- CCAGTTTGAGGTGTCTATGTC R- TCGGCGTTGTTGTAAAGC	198	55.8	F300:R200	99%
α4 nAChR	NM_015730	F-CTCAGATGTGGTCCTTGTC R- GAGTTCAGATGGGGATGCG	178	62.6	F500:R400	95%
α5 nAChR	NM_176844	F- CATCGTTTTGTTTGATAATGC R- TGCGTCCAAGTGACAGTG	90	55.8	F500:R300	84%
α6 nAChR	NM_021369	F- TGTCTCCGATCCCGTCAC R TTGTTATACAGAACGATGTCAGG	213	62.6	F600:R500	98%
α7 nAChR	NM_007390	F-GGTCATTTGCCCACTCTG R- GACAGCCTATCGGGTGAG	130	57.6	F500:R500	99%
α9 nAChR	NM_001081104	F- ACAAGGCCACCAACTCCA R- ACCAACCACTCCTCCTCTT	152	54.0	F400:R400	81%
α10 nAChR	NM_001081424	F- TCTGACCTCACAACCCACAA R- TCCTGTCTCAGCCTCCATGT	168	54.0	F500:R400	94%
β2 nAChR	NM_009602	F-CCGGCAAGAAGCCGGGACCT R- CTCGCTGACACAAGGGCTGCG	152	62.6	F300:R400	97%
β3 nAChR	NM_173212	F- AAGAAGCAGACTCCTACC R- AACAACCTGACTGATGAAG	123	62.6	F200:R600	90%
β4 nAChR	NM_148944	F- CTACAGGAAGCATTAGAGG R- CAGAATACACACAATCACG	146	50.0	F300:R200	84%
m1 mAChR	NM_007698	F-GACCCTACAGACCCCTCTCC R- CCCTTCCTCCAGTCACCAAGA	165	66.2	F600:R500	93%
m2 mAChR	NM_203491	F-CGGCTTTCTATCTGCCTGTC R- GGCATGTTGTTGTTGTTTGG	169	50.0	F100:R400	96%
m3 mAChR	NM_033269	F-GTACAACCTCGCCTTTGTTTCC R- GACAAGGATGTTGCCGATGATG	244	62.6	F400:R200	99%
m4 mAChR	NM_007699	F-GCCTTCATCCTCACCTGGAC R- AGTGGCATTGCAGAGTGCAT	146	62.6	F400:R200	99%
m5 mAChR	NM_205783	F- CCATGGACTGTGGGAAGTCA R- CAGGCGTCCCATGAGGATGTA	215	62.6	F300:R200	99%

Subunit	Accession number	Primer (5'-3')	Product (bp)	Temp (C°)	Primer ratio (nmol)	Product homology to mouse sequence
RyR3	NM_177652	**F-** AAGGTCATACTCCATCAGG **R-** AATAAGGCGGTTGTGTTC	110	50.0	F400:R200	98%

final elongation cycle. Negative controls, such as the omission of cDNA, were performed in parallel.

Optimum temperature and primer ratios were determined by selecting the conditions with the smallest Ct values that also had a melt curve containing a sharp single peak (indicating the presence of only one product). The melt peak chart was determined by plotting the negative first derivative (–dF/dt) of the relative fluorescence units versus temperature (the negative first derivative of the melt curve) using the BioRad iQ5 software. A clean melt peak chart had a single sharp peak (indicating the presence of only one product) with minimal primer dimers (the extension of self-annealed primers).

The efficiency of the reaction was determined by serial dilution of the cDNA to produce a standard curve showing the relationship between Ct and the log cDNA starting quantity. Each dilution was performed in triplicate, and standard curves were determined so that each showed a regression line with $r^2>0.95$, a slope between -3.2 and -3.5, a reaction efficiency between 95% and 105%, and an average technical error (Ct difference between replicates) less than 1 Ct. Efficiency was calculated as $10^{(-1/slope)} -1$. If the efficiency of the reaction did not fall within this range, the optimization steps were repeated until the target efficiency was obtained.

AChR whole retina qPCR experiments: Total RNA was extracted from the frozen retinas of 11 WT and 11 α7 nAChR KO mice and quality assessed following the same protocol as previously described (see RNA Extraction Protocol). RNA was extracted from the retinas of each mouse and pooled into one sample per animal. RNA was reverse transcribed and the resulting cDNA was amplified under the validated conditions. The cDNA was then diluted to a resulting concentration so that 80 ng/ul cDNA was used in each reaction. Primers for α2–α7, α9, α10, β2–β4, nAChR, and m1–m5 mAChR subunits were used; the reference gene was *RyR3*. *RyR3* was used as the reference gene because traditional housekeeping genes had too much variability between samples, and *RyR3* showed no changes in expression. The fold change was determined as previously described. The statistical significance was determined using independent sample *t* tests. The DNA products resulting from the qPCR experiments were validated by electrophoresis on a 2.5% agarose gel. PCR products were purified using the Qiaquick PCR Purification kit (Qiagen; Valencia, CA) and then sequenced to confirm their identity (Heflin Center for Genomic Sciences; University of Alabama at Birmingham; Birmingham, Al).

LCM qPCR experiments: To determine whether changes in the expressions of AChR transcripts in the whole retina varied across the layers of the retina, LCM was used to isolate cells of the outer portion of the INL (oINL), the inner portion of the INL (iINL), and the GCL. As a negative control, samples were also collected from the IPL. Samples were sectioned and prepared for LCM within 48 h of enucleation to prevent tissue degradation. To prepare for LCM, slide-mounted sections were dehydrated and processed at room temperature in sequential incubations of 75% ethanol for 30 s, two changes of RNase-free distilled water for 30 s, 75% ethanol for 30 s, 95% ethanol for 30 s, 100% ethanol for 1 min, and xylene for 5 min. The sections were dried for 5 min at room temperature and then LCD was performed using a Veritas Microdissection System (Molecular Devices; Sunnyvale, CA). For each layer (GCL, iINL, oINL), three caps containing 8–10 retinal sections were obtained for each animal. Representative images documenting laser capture were taken with the Veritas Microdissection System software. Brightness and contrast were adjusted using Adobe Photoshop; adjustments were identical for all images in a series (Adobe Systems; San Jose, CA). RNA was isolated using a Pico Pure extraction kit (Applied Biosystems; Carlsbad, CA), according to the manufacturer's protocol. RNA extracted from the three caps obtained from the same animal and capturing the same layer (GCL, iINL, or oINL) was pooled. A total of 11 WT and 11 α7 nAChR KO mice were used. Fold change, statistical significance, and DNA product validation were determined as previously described.

Western blotting: Western blotting was performed to confirm the specificity of the AChR antibodies and to confirm that proteins corresponding to the RNA transcripts were expressed. To isolate the protein, retinas were homogenized in five volumes of lysis buffer that contained 1% NP-40, 0.5% sodium deoxycholate, 0.1% sodium dodecyl sulfate, and a protease inhibitor cocktail (Sigma Aldrich; St Louis, MO). This mixture was incubated for 30 min at 4 °C and then centrifuged (Eppendorf 5810R; Westbury, NY) at 15,000 g for 20 min. The supernatant was extracted and then mixed with an equal volume of sample buffer that contained 1.0M tris-HCL, 25% glycerol, 10% SDS, 10% bromophenol blue, and 5% β-mercaptoethanol. The mixture was incubated at 95 °C for 5 min. Protein concentrations were determined using the Nanodrop ND-1000 spectrophotometer (Thermo Scientific; Wilmington, DE), and then protein samples were stored at −80 °C until use. Gel electrophoresis was used to separate protein into bands onto a 10% polyacrylamide gel. Electrophoresis was performed for 1 h at 200 V with 10–20 µg of protein. The proteins were then electrophoretically transferred to a nitrocellulose membrane using the Mini-Protean II system (Bio-Rad; Hercules, CA). Membranes were either blocked overnight at 4 °C followed by incubation with a primary antibody (Table 3) for 1 h at room temperature, or membranes were blocked for 2 h at room temperature

and incubated in a primary antibody overnight at 4 °C. The blocking solution used in both protocols was 3% non-fat dry milk (Bio-Rad; Hercules, CA) containing 1% bovine serum albumin (BSA; FisherScientific; Pittsburgh, PA) in PBS containing Tween. The membrane was then incubated in secondary antibodies and conjugated to horseradish peroxidase for 2 h. Immunoreactive bands were detected using colorimetric detection (Opti-4CN; Bio-Rad; Hercules, CA). In some cases, the signal was amplified before detection using the Western Blot Amplification Module (Bio-Rad; Hercules, CA). All controls were performed in parallel with experimental conditions. To ensure primary antibody specificity, we used matched concentrations of the protein immunoglobulin G (IgG) from the animal in which the primary antibody was made. To control for secondary antibody specificity, the primary antibody was omitted and membranes were incubated in a blocking medium instead of a primary antibody.

IHC: Retinas from a total of 5 WT and 5 α7 nAChR KO mice were used in CHAT wholemount IHC. Retinas to be used for ChAT (Millipore, Billerica, MD) wholemount IHC were processed by free-floating following isolation from the choroid and the sclera. Retinas were washed in four changes of 0.1 M PBS, incubated in 10% donkey serum (DKNS; Jackson Immunoresearch; Westgrove, PA), and diluted in PBS/0.03% Triton-X for 24 h at 4 °C. Retinas were then incubated in ChAT with 10% DKNS and 0.3% sodium azide in PBS/0.03% Triton-X for 11 days at 4 °C, washed in four changes of 0.1M PBS, incubated in fluorescein-conjugated-donkey-anti-goat (Jackson Immunoresearch; Westgrove, PA) and in 0.3% sodium azide/PBS/0.03% Triton-X for 72 h at 4 °C, mounted, and stored at 4 °C until imaging. Images were collected with a Leica TCS SP confocal laser

scanning microscope. Brightness, contrast adjustments, and figure preparations were completed in Adobe Photoshop (Adobe Systems; San Jose, CA). For each retina, cell counts were obtained from five optical z-stack confocal sections taken under 40X magnification in the INL and GCL, respectively. Regions of interest were non-overlapping 500 μm by 500 μm areas approximately 500 μm away from the optic nerve [54], and cells were counted using a colony counter pen (Research Products International; Mount Prospect, IL). Total retinal cell counts were the sum of the INL and GCL counts. Student *t* tests were performed to determine whether there were differences in cell counts between the INL and the GCL in both WT and α7 nAChR KO mice. Student *t* tests were also performed to determine whether there was a difference in cell counts between WT and α7 nAChR KO mice in the INL, the GCL, or the total retina.

Eyecups to be used for vertical IHC double label experiments were fixed by immersion in 1% PLP for 2 h at room temperature. Eyecups were then cryoprotected by sequential immersion in 0.1 M PBS with graded concentrations of sucrose (10%, 20%, and 30%) for 30 min each and then stored at 4 °C. For cryosectioning, eyecups were embedded in a block of 50% optimum cutting temperature medium (Sakura Finetek, Torrance, CA) and 50% aquamount (VWR Scientific; West Chester, PA), frozen, sectioned into 10−12μm vertical cryosections (Leica CM 3050), mounted onto superfrost slides (VWR Scientific; West Chester, PA), and stored at −20 °C.

Immediately before use, the sections were warmed for 45 min and washed in three changes of 0.1 M PBS. All sections were then incubated in 10% DKNS (Jackson Immunoresearch) for 1 h at room temperature, followed by incubation

Antibody (antigen)	Species	Catalog No.	Supplier
α1, α3, α5 nAChR A synthetic peptide corresponding to the main immunogenic region on the extracellular surface of muscle α1 AChR subunit, as well as the α3 and α5 subunits of human neuronal AChRs. The antibody binds the α1 subunit weakly when the protein is denatured, but can only detect the α3 and α5 subunit in native forms.	rat	mAb 210 (1:200 IHC)	Gift of Dr Jon Lindstrom, University of Pennsylvania
	rat	AB24719 (1:1000 Western)	Abcam, Cambridge MA
α9 nAChR A synthetic peptide corresponding to the N-terminal region of the human nAChR α9 protein.	rabbit	AB49065 (1:100 IHC) (1:1000 Western)	Abcam, Cambridge MA
m1 mAChR A Glutathione S-transferase (GST) fusion protein corresponding to a part of the i3 intracellular loop of human m1 mAChR protein (227–353).	rabbit	AB5164 (1:100 IHC) (1:50 Western)	Chemicon, Temecula CA
m2 mAChR A GST fusion protein corresponding to a part of the i3 intracellular loop of the m2 receptor (225–359).	rat	mAB367 (1:100 IHC) (1:100 Western)	Chemicon, Temecula CA
Choline Acetyltransferase/ChAT Protein corresponding to the human placental enzyme.	goat	AB144P (1:200 IHC)	Chemicon, Temecula CA

TABLE 3. ANTIBODIES AGAINST ACETYLCHOLINE RECEPTORS

overnight in a primary antibody at 4 °C (Table 3). They were then washed again in three changes of 0.1 M PBS, incubated for 1 h with the secondary antibody that was conjugated to a fluorescent dye, washed again, and then incubated in a ChAT primary antibody overnight at 4 °C. Sections were then washed again, incubated for 1 h with the secondary antibody that was conjugated to a different fluorescent dye, washed again, coverslipped, and stored at 4 °C until imaging. Appropriate controls included the substitution of matched IgG protein concentrations for the primary antibodies and the omission of primary antibodies. Antibodies were obtained from Abcam (Cambridge, MA), Chemicon (Billerica, MA), and Santa Cruz (Santa Cruz, CA). The mAb 210 antibody was generously provided by Dr. Jon Lindstrom (University of Pennsylvania). Secondary antibodies were raised in donkey and obtained from the Jackson Immunoresearch Laboratories (West Grove, PA).

Images of vertical IHC were collected with a Leica TCS SP confocal laser scanning microscope. Each image was composed of six sequential sections. Brightness and contrast were adjusted using Adobe Photoshop (Adobe Systems; San Jose, CA), and adjustments were applied identically for all images for each antibody.

RESULTS

qPCR SuperArray screening: To assess changes in the expressions of many different candidate genes at one time, qPCR custom SuperArrays were designed. SuperArrays included primers for a wide variety of targets, including the members of the ligand gated ion channel superfamily and receptors that activate the same protein cascades as mAChRs (Table 1). The qPCR screening results indicated a significant 1.19 (SEM = 0.082)-fold upregulation (t [14] = −2.200, p<0.05) of the β2 GABA$_A$ receptor subunit, indicating that the β2 GABA$_A$ transcript expression was significantly higher in the KO mice than in the WT mice. There was also a significant −1.50 (SEM = 0.182)-fold downregulation (t [14] = 2.290, p<0.05) of the α5 nAChR subunit RNA transcript, a −1.78 (SEM = 0.252)-fold downregulation (t [12] = 2.185, p<0.05) of the m1 mAChR subtype RNA transcript, and a −1.98 (SEM = 0.225)-fold downregulation (t [12] = 2.884, p<0.05) of the inwardly rectifying potassium, subfamily J, member 4 channel (Kcnj4) RNA transcript. These data indicate that the α5 nAChR, m1 mAChR, and Kcnj4 targets were significantly downregulated in KO mice relative to WT mice (Figure 1). ChAT, the rate-limiting step in ACh synthesis, is regularly used as a marker for sites of ACh synthesis and release. To assess whether the compensation for the lack of α7 nAChRs was mediated by changes in the overall levels of ACh, ChAT

was also included in the SuperArray. However, there was no change in the mRNA expression of ChAT in the α7 nAChR KO mice, as compared to the WT mice. This suggests that the rate of ACh synthesis was not altered in the α7 nAChR KO mice. As the primer sets in PCR arrays are proprietary, the primer sequences were unavailable for use in obtaining product sequences. We chose to focus on the nAChR transcript expression to test our prediction that changes in other AChR subunits or subtypes were compensatory.

Whole retina AChR qPCR: To assess changes in the mRNA expressions observed using the SuperArrays and to confirm the product homology to the targeted mouse DNA sequence, custom primers for AChRs, designed against mouse sequences, were optimized for qPCR. The resulting qPCR products were subjected to electrophoresis on a 2.5% agarose gel, and single bands of the expected molecular weight were obtained (Figure 2). Products were sequenced and then compared to published sequences using the standard nucleotide BLAST. PCR product homology to mouse nAChR and mAChR DNA ranged from 81–100% (Table 2). The qPCR results, using RNA extracted from WT and α7 nAChR KO mouse retinas (Figure 3), indicated a significant 3.11-fold upregulation (t [16] = −4.280, p<0.001; SEM = 0.263) of the α2 nAChR subunit, a 3.5-fold upregulation (t [15] = −2.118, p<0.05; SEM = 0.586) of the α9 nAChR subunit, a 2.66-fold upregulation (t [18] = −1.831, p<0.05; SEM = 0.553) of the α10 nAChR subunit, a 1.49-fold upregulation (t [18] = −3.693, p<0.001; SEM = 0.107) of the β4 nAChR subunit, a 3.8- fold upregulation (t [18] = −2.087, p<0.05; SEM = 0.627) of the m1 mAChR subtype, and a 6.22-fold upregulation (t [15] = −2.941, p<0.01; SEM = 0.589) of the m4 mAChR subtype. Results also indicated a significant −2.95-fold downregulation (t [16] = 1.768, p<0.05; SEM = 0.582) of the α5 nAChR subunit. Because α9 and α10 nAChR transcripts have not been previously reported in retinas, and to further confirm primer specificity, we tested our primers using retinal mRNA obtained from α7 nAChR KO, α9 nAChR KO, and α10 nAChR KO mouse retinas. No α7 nAChR transcripts were amplified from RNA extracted from α7 nAChR KO mouse retinas when qPCR was performed using the α7 nAChR primer set. No α9 nAChR transcripts were amplified from RNA extracted from α9 nAChR KO mouse retinas when qPCR was performed using the α9 nAChR primer set. Similarly, no α10 nAChR transcripts were amplified from RNA extracted from α10 nAChR KO mouse retinas when qPCR was performed using the α10 nAChR primer set (not shown).

LCM: To determine whether the AChR expressions varied among the different retinal cell populations, LCM was used to extract cells from the GCL, the iINL, and the oINL. The
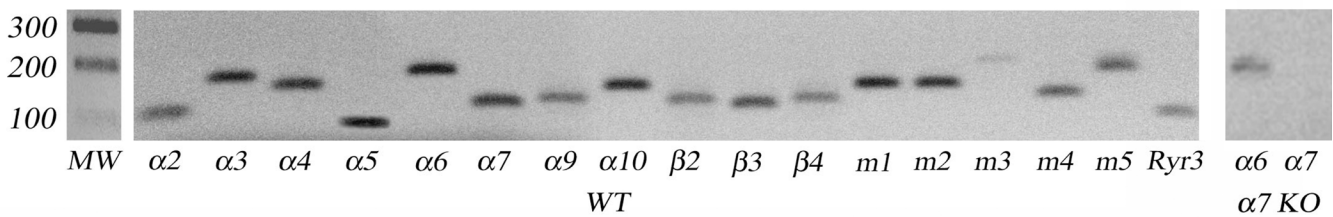
Figure 2. 2.5% agarose gel of the acetylcholine receptor qPCR products. (Left) Products obtained from wild-type (WT) mouse retinal RNA extracts using custom-designed primers for α2–α7, α9, α10, and β2–β4 nAChR subunits as well as m1–m5 mAChR subtypes are shown. Products (Right) obtained from α7 nAChR knockout (KO) mouse retinal RNA extracts using primers for α6 and α7 nAChR subunits. Each qPCR product has a single band of the expected size. As expected, there is no band present for the qPCR product from the reaction containing the α7 nAChR primer and the α7 nAChR KO mRNA. *p<0.05, (n=8).

GCL is composed of ganglion and displaced amacrine cell populations. The iINL is composed of primarily amacrine and a few bipolar cells, while the oINL is composed of horizontal and bipolar cells. Representative images of the retinal tissue before and after each laser capture are shown in Figure 4. Retinal layers were distinguishable and could be reliably captured. Tissue was also collected from the IPL (image not shown) as a negative control. As expected, the mRNA transcripts were not amplified from this synaptic layer.

LCM qPCR–nAChR α subunits: The α2 nAChR subunit transcripts were upregulated in the whole retina, but downregulated in the GCL and the INL (Figure 5). Specifically, qPCR results indicated a significant 3.11-fold (SEM = 0.263) upregulation (t [16] = −4.280, p<0.001) of the α2 nAChR
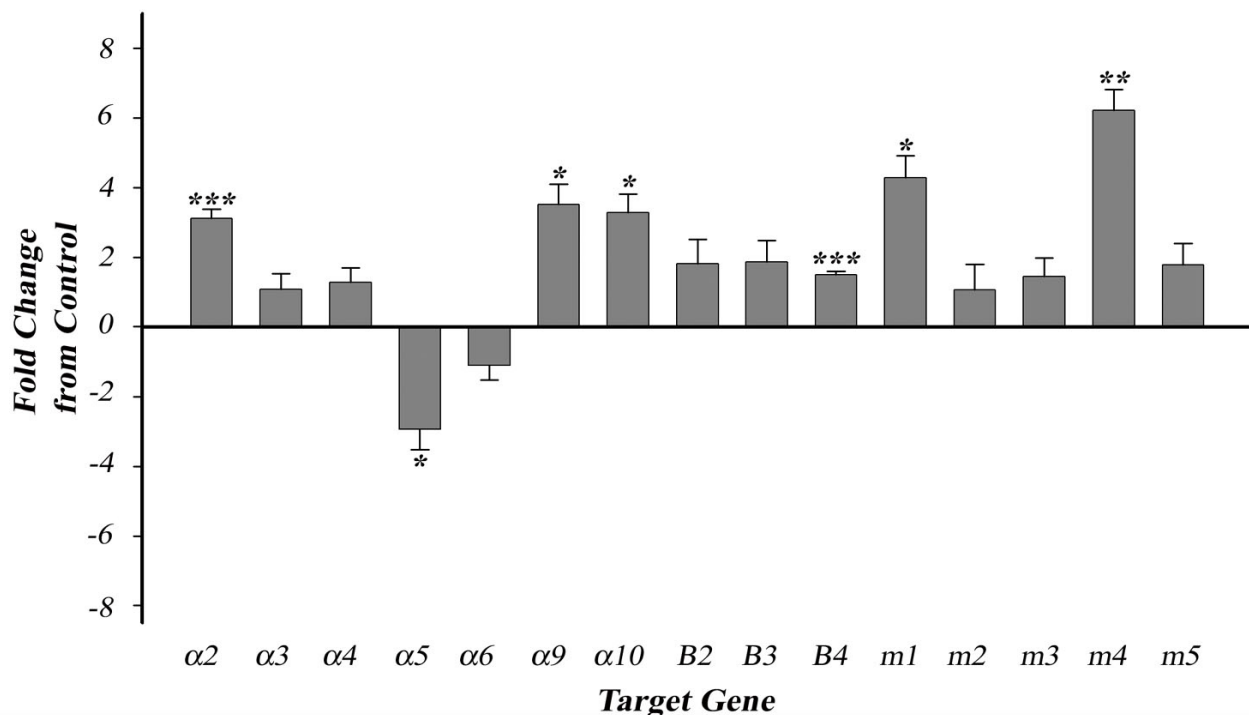
Figure 3. Acetylcholine receptor qPCR fold changes in a whole mouse retina. The qPCR showed a significant upregulation of the α2, α9, α10, and β4 nAChR subunits or the m1 and m4 mAChR subtypes. There was also a significant downregulation of the α5 nAChR subunit. Error bars represent the SEM. *p<0.05, **p<0.01, ***p<0.001, (n=11).
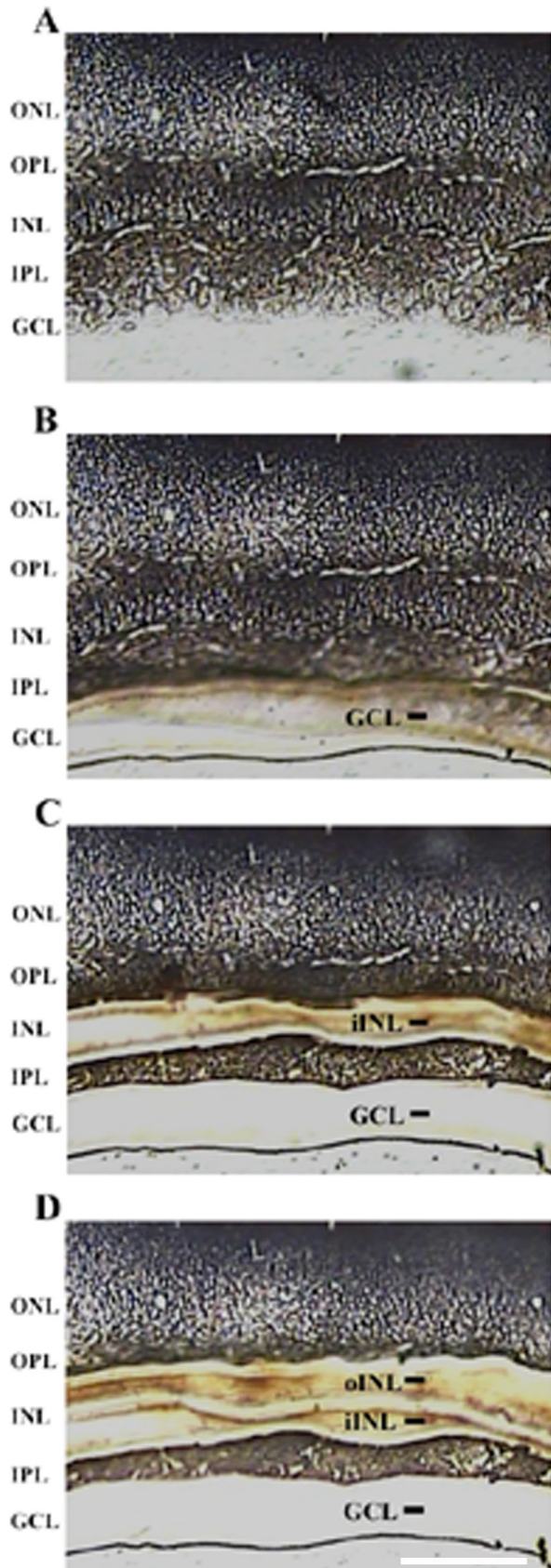
Figure 4. Images of vertical sections depicting laser capture microdissection (LCM) of the unfixed mouse retinas. Vertical section of an unfixed mouse retina. **A**: before LCM; **B**; after dissection of the ganglion cell layer (GCL–); **C**: after dissection of the GCL and the inner portion of the inner nuclear layer (iINL–), and **D**: after dissection of the GCL, the iINL, and the outer portion of the inner nuclear layer (oINL–). Scale bar, 100 μm.

subunit in the whole retina. None of the captured regions of the retina showed upregulation of the α2 nAChR subunit transcript. Instead, there was a significant −3.0-fold (SEM = 0.504) downregulation (t [13]= 2.243 p<0.05) in the iINL.

Furthermore, the α5 nAChR subunit transcripts were downregulated in the whole retina and in the inner retina. There was a significant 2.95-fold (SEM = 0.582) downregulation (t [16] = 1.768, p<0.05) of the α5 nAChR subunit transcripts in the whole retina and a non-significant trend toward downregulation in the oINL, the iINL, and the GCL.

The α9 nAChR subunit transcription was upregulated in the whole retina, the GCL, and the oINL, and it was significantly downregulated in the iINL. There was a significant 3.5-fold (SEM = 0.586) upregulation (t [18] = −1.831, p<0.05) of the α9 nAChR subunit transcripts in the whole retina and a non-significant trend toward upregulation in the oINL and the GCL. There was a significant −6.26-fold (SEM = 0.575) downregulation (t [14] = 3.521, p<0.01) of the α9 nAChR subunit transcripts in the iINL.

Finally, α10 nAChR subunit transcripts were upregulated in the whole retina, the oINL, and the GCL, and they were downregulated in the iINL. There was a 2.66-fold (SEM = 0.553) upregulation (t [18] = −1.831, p<0.05) of the α10 nAChR subunit transcripts in the whole retina, a non-significant trend toward upregulation in the oINL and the GCL, and a non-significant trend toward downregulation in the iINL.

LCM qPCR–nAChR β subunits: The β2 nAChR subunit transcripts were upregulated in the oINL, but they trended toward downregulation in the whole retina, the iINL, and the GCL. Specifically, there was a non-significant trend toward an upregulation of the β2 nAChR subunit transcripts in the whole retina. There was a significant 3.36-fold (SEM = 0.379) upregulation (t [17] = −3.218, p<0.01) of the β2 nAChR subunit transcripts in the oINL, as well as a non-significant trend toward downregulation in the iINL and the GCL.

The β3 nAChR subunit transcripts were downregulated in the GCL, and they trended toward downregulation in the INL and toward upregulation in the whole retina. There was a non-significant trend toward an upregulation of the β3 nAChR subunit transcripts in the whole retina. Conversely, there was a statistically significant −2.54-fold (SEM = 0.246) downregulation (t [19] = 3.844, p<0.001) of the β3 nAChR subunit transcripts in the GCL and a non-significant trend toward downregulation in the INL.

Finally, β4 nAChR subunit transcripts were upregulated in the whole retina and the oINL but downregulated in the iINL and the GCL. There was 1.49-fold (SEM = 0.107) upregulation (t [18] = −3.693, p<0.001) of the β4 nAChR subunit

transcripts in the whole retina and a 1.15-fold (SEM = 0.079) upregulation (t [20] = −1.751, p<0.05) in the oINL. There was a significant −1.60-fold (SEM = 0.067) downregulation (t [18] = −2.087, p<0.001) of the β4 nAChR subunit transcripts in the iINL and a 2.90-fold (SEM = 0.097) downregulation (t [19] = 11.060, p<0.001) in the GCL.

LCM qPCR–mAChR subtypes: The m1 mAChR subtype transcripts were upregulated in the whole retina, the oINL, and the GCL, and they were downregulated in the iINL. Specifically, there was a significant 3.81-fold (SEM = 0.627) upregulation (t [18] = −2.087, p<0.05) of the m1 mAChR subtype transcripts in the whole retina, with a non-significant trend toward upregulation in the oINL and the GCL and a non-significant trend toward downregulation in the iINL. The m2 mAChR subtype transcripts were upregulated in the whole retina and the GCL, and they were downregulated in the INL. There was a non-significant trend toward upregulation of the m2 mAChR subtype transcripts in the whole retina and a significant 5.58-fold (SEM = 0.335) upregulation (t [10] = −5.234, p<0.001) in the GCL. However, there was also a non-significant trend toward downregulation in the oINL and a significant −5.08-fold (SEM = 0.637) downregulation (t [18] = 2.604, p<0.01) in the iINL. Finally, m4 mAChR subtype transcripts were upregulated in the whole retina, the oINL, and the GCL, but they were downregulated in the iINL. There was a significant 6.22-fold (SEM = 0.589) upregulation (t [15] = −2.941, p<0.01) of the m4 mAChR subtype transcripts in the whole retina, a 2.48-fold (SEM = 0.502) upregulation (t [9] = −1.885, p<0.05) in the oINL, and a 2.63-fold (SEM = 0.289) upregulation (t [10] = −3.415, p<0.01) in the GCL. However, there was also a significant −2.00-fold (SEM = 0.311) downregulation (t [14] = 2.268, p<0.05) of the m4 mAChR subtype transcripts in the iINL.

LCM qPCR–retinal layers: The qPCR results, obtained using RNA extracted from the different retinal layers, indicated that some AChR subunits and subtypes were both up- and downregulated, depending on the region within the retina (Figure 6). The qPCR results, obtained using RNA extracted from the oINL, indicated significant upregulation, as well as trends toward up- and downregulation for AChR subunits and subtypes. In addition, qPCR results, obtained using RNA extracted from the iINL, exhibited significant downregulation but no upregulation or trends toward upregulation. Finally, qPCR results, obtained using RNA extracted from the GCL, showed significant up- and downregulation.

Western blotting: Western blot analyses were performed using antibodies against the AChR subunits and subtypes that were differentially regulated between WT and α7 nAChR KO mice. Protein used in western blotting was extracted from
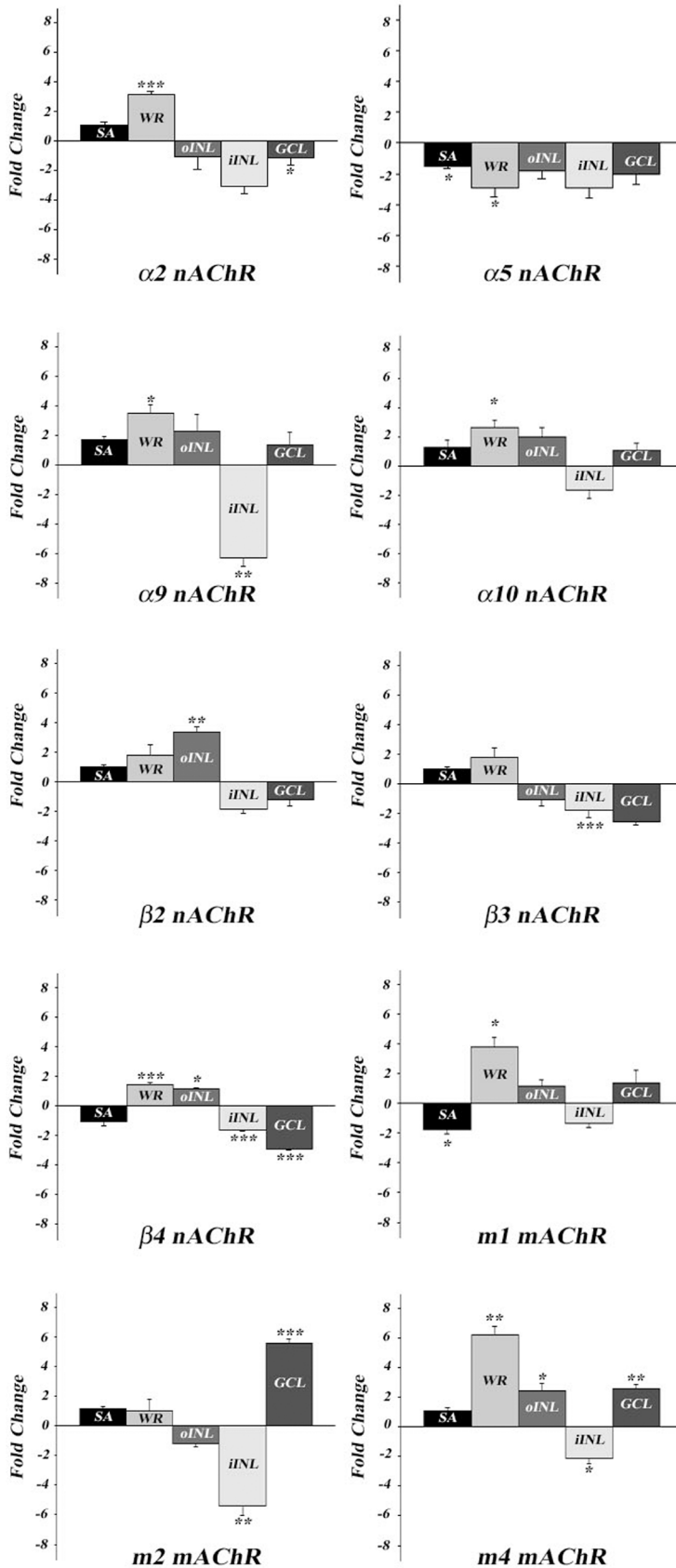
Figure 5. A comparison of significant qPCR targets across experiments. The α2 nAChR subunits were upregulated in the whole retina and downregulated in the GCL. The α5 nAChR subunits were downregulated in the whole retina using either superarray (SA) or designed primers. The α9 nAChR subunits were upregulated in the whole retina and downregulated in the iINL. The α10 nAChR subunits were upregulated in the whole retina. The β2 nAChR subunits were upregulated in the oINL. The β3 nAChR subunits were downregulated in the iINL. The β4 nAChR subunits were upregulated in the whole retina and the oINL and downregulated in the iINL and the GCL. The m1 mAChR subtypes were upregulated in the whole retina using designed primers and downregulated using SA primers. The m2 mAChR subtypes were upregulated in the GCL and downregulated in the iINL. The m4 mAChR subtypes were upregulated in the whole retina, the oINL, and the GCL and downregulated in the iINL. SA- SuperArray, WR- whole retina, oINL- outer portion of INL, iINL- inner portion of INL, GCL- ganglion cell layer, Error bars represent SEM. ***p<0.001, SA (n=8), WR (n=11), LCM (n=11).
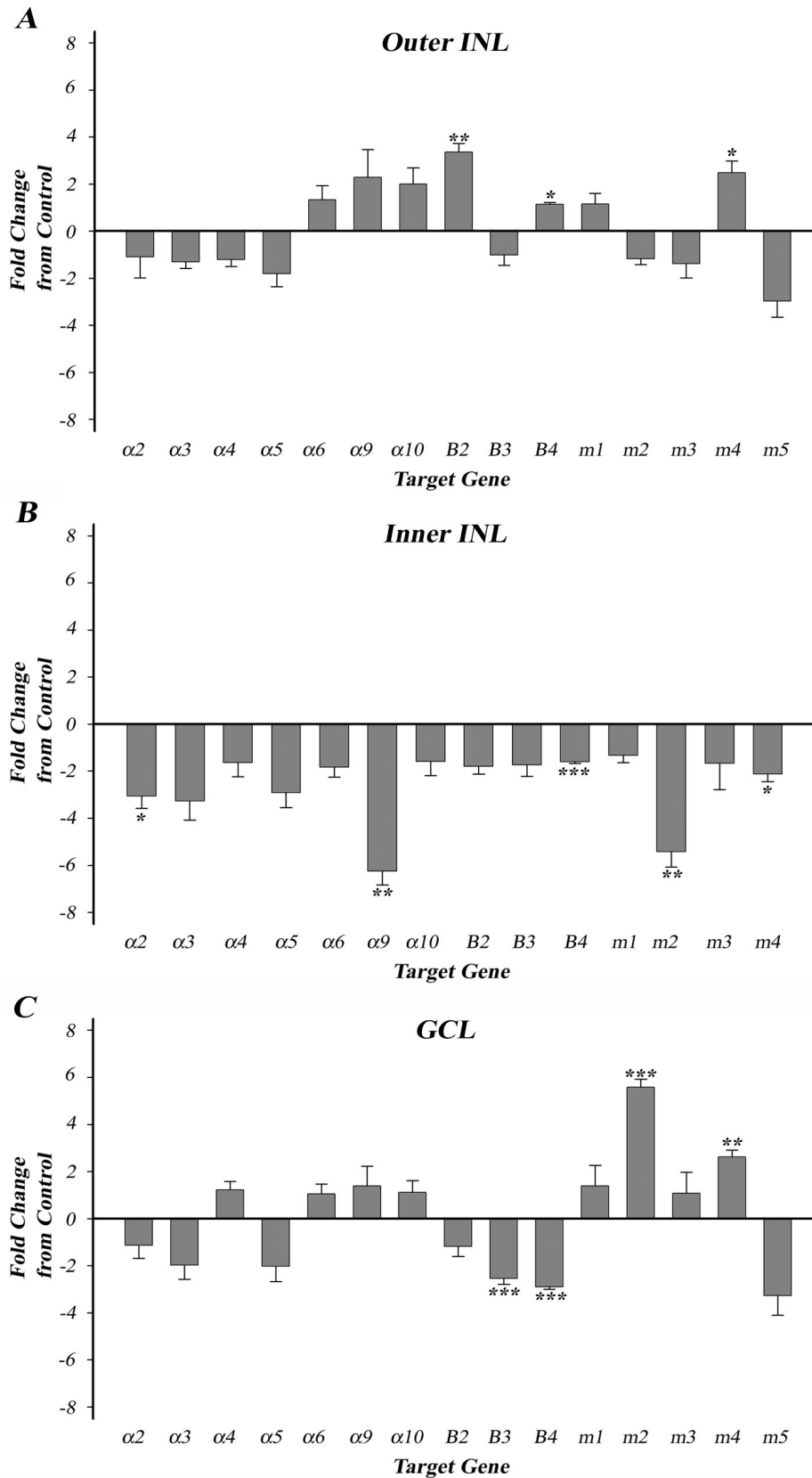
Figure 6. Acetylcholine receptor qPCR fold changes in the oINL, the iINL, and the GCL of the mouse retinas. **A**: In the oINL, there was an upregulation of the β2 and β4 nAChR subunits. **B**: In the iINL, there was a downregulation of the α2, α9, and β4 nAChR subunits as well as the m2 and m4 mAChR subtypes. All acetylcholine receptor (AChR) subunits and subtypes showed downregulation or trended toward downregulation in the iINL. **C**: In the GCL, there was an upregulation of the m2 and m4 mAChR subtypes and an upregulation of the β3 and β4 nAChR subunits. Error bars represent SEM. *p<0.05, **p<0.01, ***p<0.001, (n=11).

whole mouse retinas. Western blot analyses with antibodies against mAChR subtypes and nAChR subunits resulted in a single band of the size predicted by the Universal Protein Resource (UniProt) protein sequence database (Figure 7A, Table 3). Other antibodies did not yield a single band of the predicted size and so were not used for subsequent IHC analyses. A single 51 kDa band was visualized for AB24719, an antibody that recognizes the epitope corresponding to the main immunogenic region on the extracellular surface of the human muscle α1 nAChR as well as the α3 and α5 neuronal nAChR subunit proteins [24,25]. A single 53 kDa band was visualized for AB49065, an antibody that recognizes the epitope corresponding to the N-terminal regions of the human α9 nAChR protein. A single 60 kDa band was visualized for AB5164, an antibody that recognizes the epitope corresponding to amino acids 227–353 of the human m1 mAChR protein. A single 52 kDa band was visualized for mAB367, an antibody that recognizes the epitope corresponding to amino acids 225–359 of the human m2 mAChR protein. The western blot data confirmed antibody specificity and indicated the presence of the α3−α5 and α9 nAChR subunits, as well as the m1 and m2 mAChR subtype proteins in mouse retina, and it confirmed antibody specificity. Primary antibody omission and IgG controls yielded no bands (Figure 7B). As this is the first report of α9 nAChR protein expressions in mouse retina, we tested the specificity of the antibody with protein from α9 nAChR KO mouse retinas. Western blots obtained using protein extracted from α9 nAChR KO mouse retinas yielded no bands when probed using antibodies against the α9 nAChR subunit.

Antibodies made against α2, α3, α6, or α10 nAChRs were also tested (not shown), but each of the antibodies tested yielded multiple bands on westerns, indicating a potential lack of specificity and they were excluded from this study. Furthermore, consistent with previous reports, commercially available antibodies against α7 nAChRs yielded labeling patterns in α7 nAChR KO mouse retinas similar to those seen in WT mouse retinas, or they yielded no specific labeling; therefore, α7 nAChR antibodies were not used in this study [55]. This does not suggest that α2, α6, α7, and α10 nAChR subunits are absent from mouse retina but instead is simply the result of a lack of specific antibodies.

ChAT wholemount IHC: To assess whether an absence of α7 nAChRs correlated with the changes in the number of cholinergic amacrine cells, we also assessed the distribution and number of ChAT immunoreactive cells in the WT and the α7 nAChR KO mouse retinas. A change in the number of ChAT immunoreactive cells might indicate a change in the overall levels of ACh. The distribution of ChAT immunoreactivity in

the WT mice has been previously described and our studies yielded similar results in both the distribution and number of cells. ChAT immunoreactivity was displayed by a subset of amacrine cells in the INL and a population of displaced amacrine cells in the GCL, with two well-labeled bands of dendrites in the second and fourth sublamina of the IPL [56,57]. In the central WT mouse retina, the INL contained, on average, 1,390.6 per mm^2 (SD = 162.14) ChAT immunoreactive amacrine cells, which was significantly higher than the GCL, which contained, on average, 1,016.8 per mm^2 (SD = 75.79) ChAT immunoreactive amacrine cells (Figure 8). Similarly, in the central α7 nAChR KO mouse retina, the INL contained, on average, 1,349.33 per mm^2 (SD = 61.49) ChAT immunoreactive amacrine cells, which was significantly higher than the GCL, which contained, on average, 1,142.67 per mm^2 (SD = 73.22) ChAT immunoreactive amacrine cells. A higher number of ChAT immunoreactive cells in the INL compared to the GCL was observed in both WT (t [8]= –2.987, p<0.05) and α7 nAChR KO (t [8]= –9.519, p<0.001) mice. In both the INL and the GCL, there were no significant differences in the number or distribution patterns of ChAT immunoreactive cells in the α7 nAChR KO mice as compared to the WT mice. Thus, the absence of α7 nAChRs did not appear to affect the cholinergic cell populations. Therefore, changes in the expressions of nAChR subunits or mAChR subtypes in α7 nAChR KO mice were not likely due to changes in the number and distribution of ChAT-containing amacrine cells.

nAChR/ChAT double label IHC: Protein expression patterns for ChAT plus α3/α5 or α9 nAChR subunits in WT and α7 nAChR KO mouse retinas were assessed. Because there were no differences in the ChAT mRNA or the protein expressions between WT and α7 nAChR KO mouse retinas, ChAT immunoreactivity was used to normalize the brightness and contrast for IHC images as a positive control to ensure experimental consistency and to delineate IPL sublamina within the retina.

Presumptive amacrine, bipolar, and ganglion cells displayed mAb210 immunoreactivity (Figure 9), as mAb210 is an antibody that specifically labels α3 and α5 nAChR subunits in the retina [24,25]. It also recognizes the main immunogenic region on the extracellular domain of the muscle α1 nAChR, but the α1 subunit is not thought to be expressed by the neuronal tissue [24]. Furthermore, mAb210 immunoreactivity in cell bodies was restricted to what appeared to be a thin layer of cytoplasm surrounding the nucleus, probably indicating the presence of α3 and α5 nAChRs that were synthesized but not yet transported to synaptic zones. Dendrites that displayed immunoreactivity
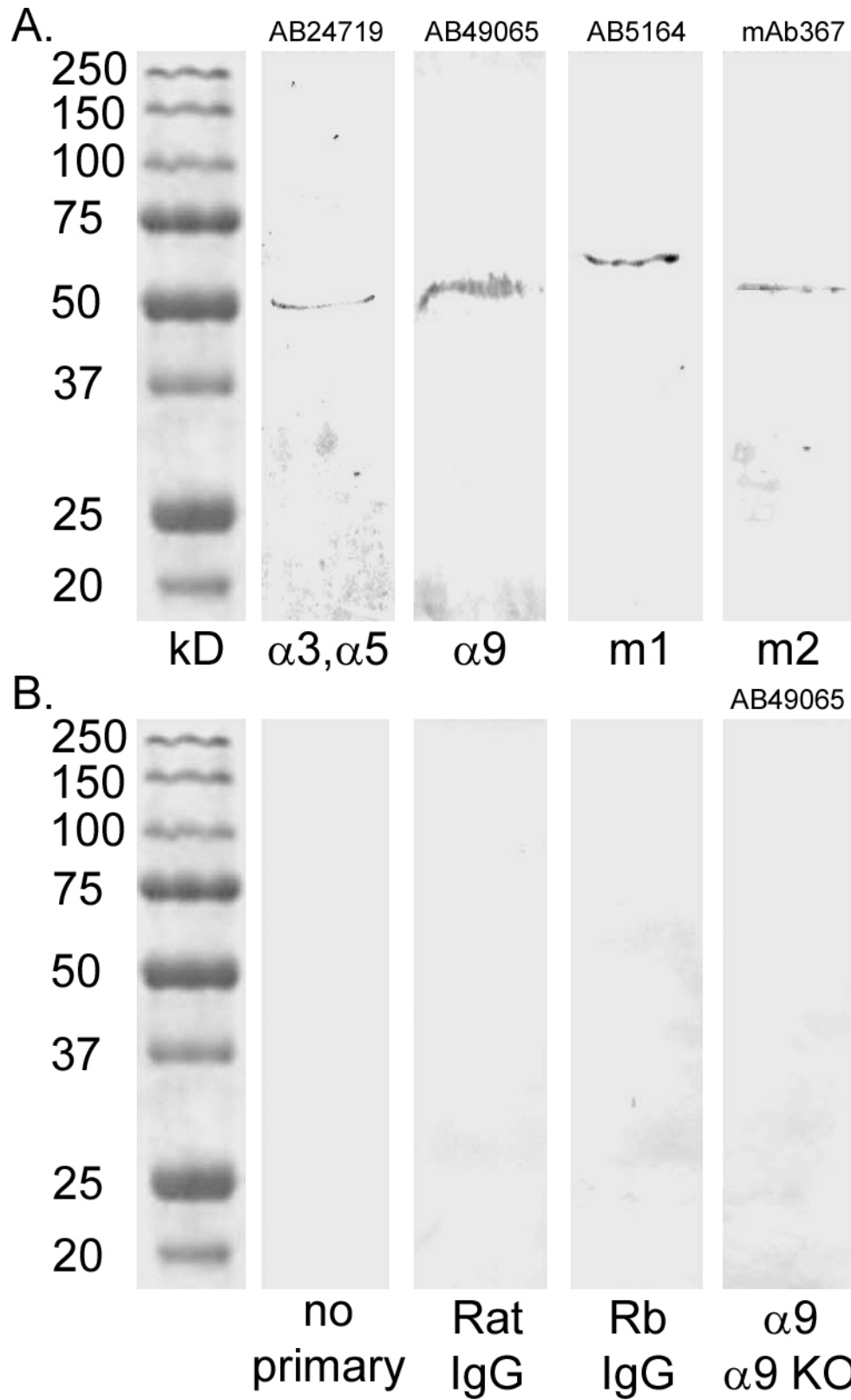
Figure 7. Western blot analyses with antibodies against acetylcholine receptors. Protein extracts from WT C57BL/6J mouse retina. **A**: Western blots obtained had a single band at the predicted molecular weight. This confirmed the presence of the nAChR subunit and mAChR subtype protein and antibody specificity. Blots for each antibody were obtained separately and compiled for the figure. α1, α3, α5 (AB24719-Rat) 51 kDa; α9 nAChR (AB49065-Rb), 53 kDa; m1 mAChR (AB5164-Rb), 60 kDa; m2 mAChR (mAB367-Rat), 52 kDa. **B**: Representative western blots for control conditions; clean, with no bands present. IgG: Immunoglobulin G; Rb: Rabbit.
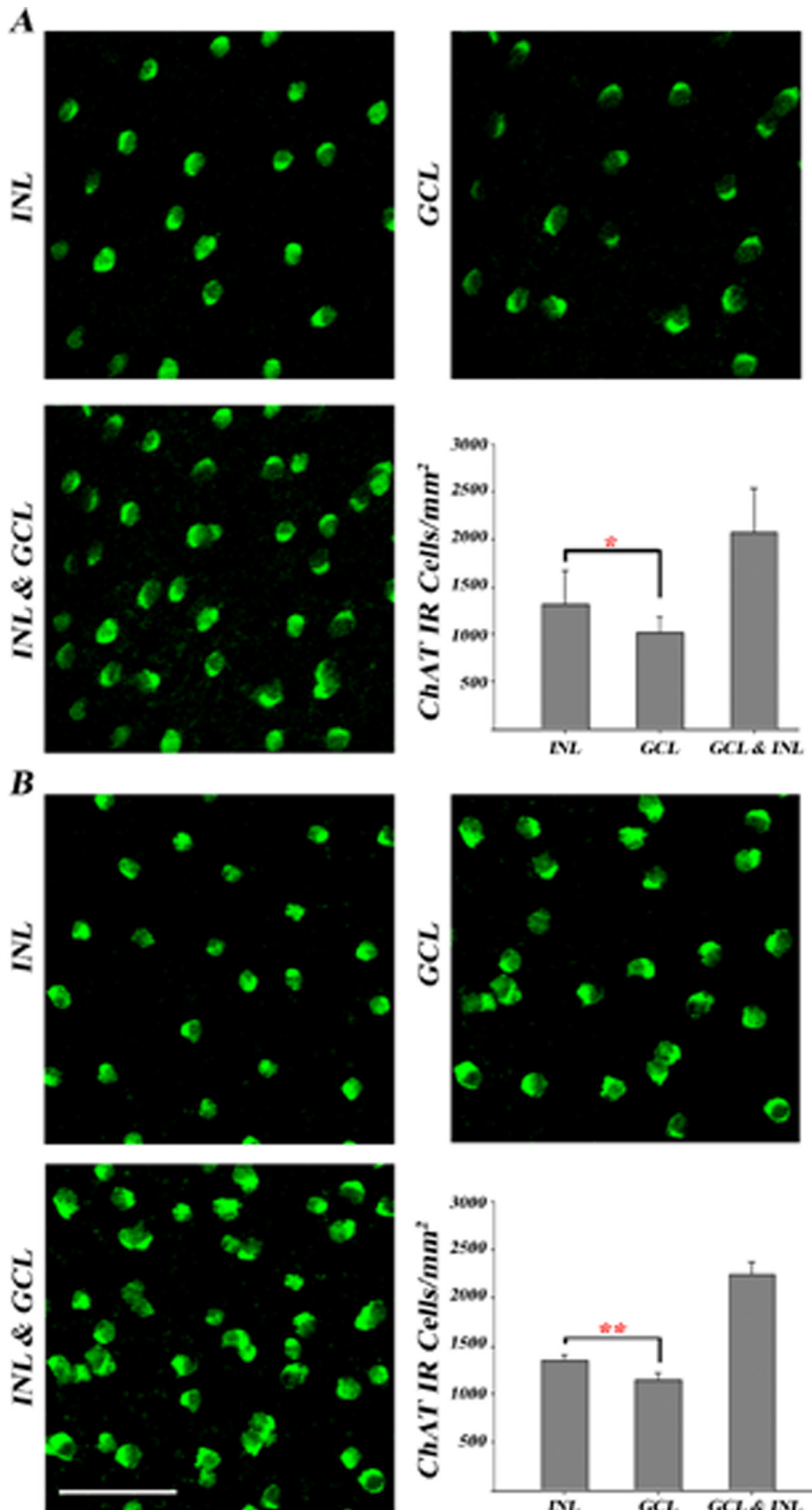
Figure 8. Wholemount choline acetyltransferase (ChAT) immunohistochemistry (IHC). There was a significant increase in the number of ChAT immunoreactive amacrine cells in the inner nuclear layer (INL) compared to the GCL in both **A**: WT C57BL/6J mice, *p<0.05 (n=5) and **B**: α7 nAChR KO mice, **p<0.001 (n=5). Error bars represent SEM. There was no significant difference between WT and α7 nAChR KO mice. For each retina, cell counts were obtained from five optical z-stack confocal sections taken under 40X magnification in the INL and the GCL, respectively. Regions of interest were non-overlapping 500 μm by 500 μm areas approximately 500 μm away from the optic nerve. Scale bar, 50 μm.

for mAb210 were broadly distributed through the IPL and overlapped the ChAT immunoreactive processes in sublamina 2 and sublamina 4, suggesting that α3 and α5 nAChRs are distributed on processes within the ON and OFF pathways. A thin band at sublamina 3 of the IPL was not mAb210 immunoreactive, suggesting that a specific population of cells that stratify at the margins of the ON and OFF sublamina do not express α3 and α5 nAChRs. In addition, faint mAb210 immunoreactivity was observed at the level of the outer plexiform layer (OPL), probably from the processes of labeled bipolar cells. Similar patterns of immunoreactivity were observed in the α7 nAChR KO mouse retinas, but the labeling was less intense than in the WT mice when images were taken using identical settings for image capture. This is consistent

with mRNA results showing a downregulation of α5 nAChR subunits in the α7 nAChR KO mouse retina.

Immunoreactivity for AB49065, an antibody specific for α9 nAChRs, was distributed in a variety of cell types, including presumptive amacrine, bipolar, and ganglion cells, as well as throughout the IPL (Figure 10). As was observed with mAb 210 labeling, immunoreactivity in cell bodies was restricted to what appeared to be a thin layer of cytoplasm surrounding the nucleus, indicating the presence of α9 nAChRs synthesized but not yet transported to synapses. There appeared to be fewer cell bodies labeled in the α7 nAChR KO mouse retina, and α9 nAChR immunoreactivity was broadly distributed through the IPL and encompassed
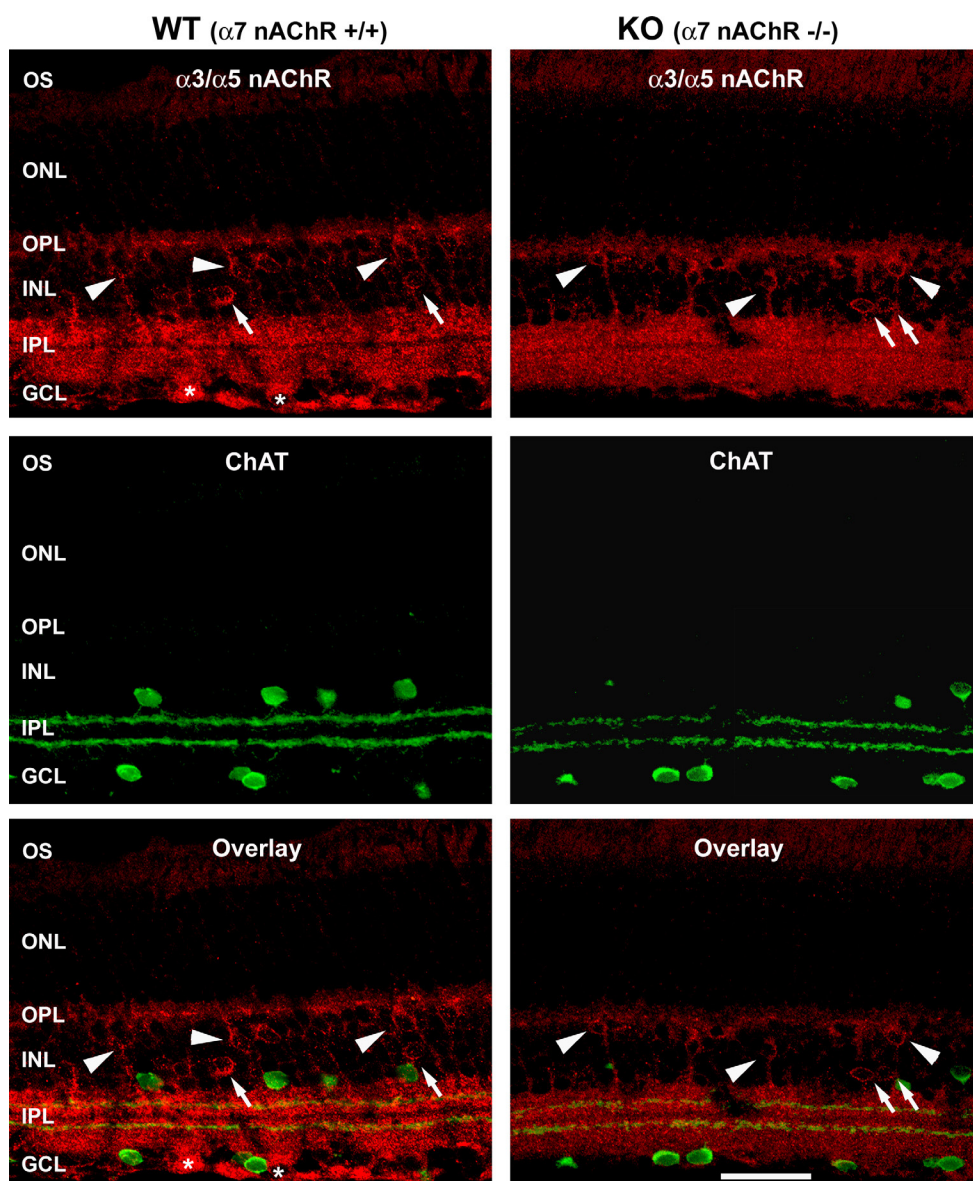

Figure 9. nAChR IHC in α7 nAChR KO and WT mouse retinas. (**A**) Labeling patterns of the α3/α5 nAChR antibody (red) revealed labeling in the amacrine (arrows), bipolar (arrowheads), and ganglion cells (asterisks) in both the WT and α7 nAChR KO mouse retinas, with less intense labeling in the KO mouse retinas. Inner plexiform layer (IPL) immunoreactivity encompassed ChAT (green) immunoreactive IPL bands, but there were no double labeled ChAT-positive cell bodies.
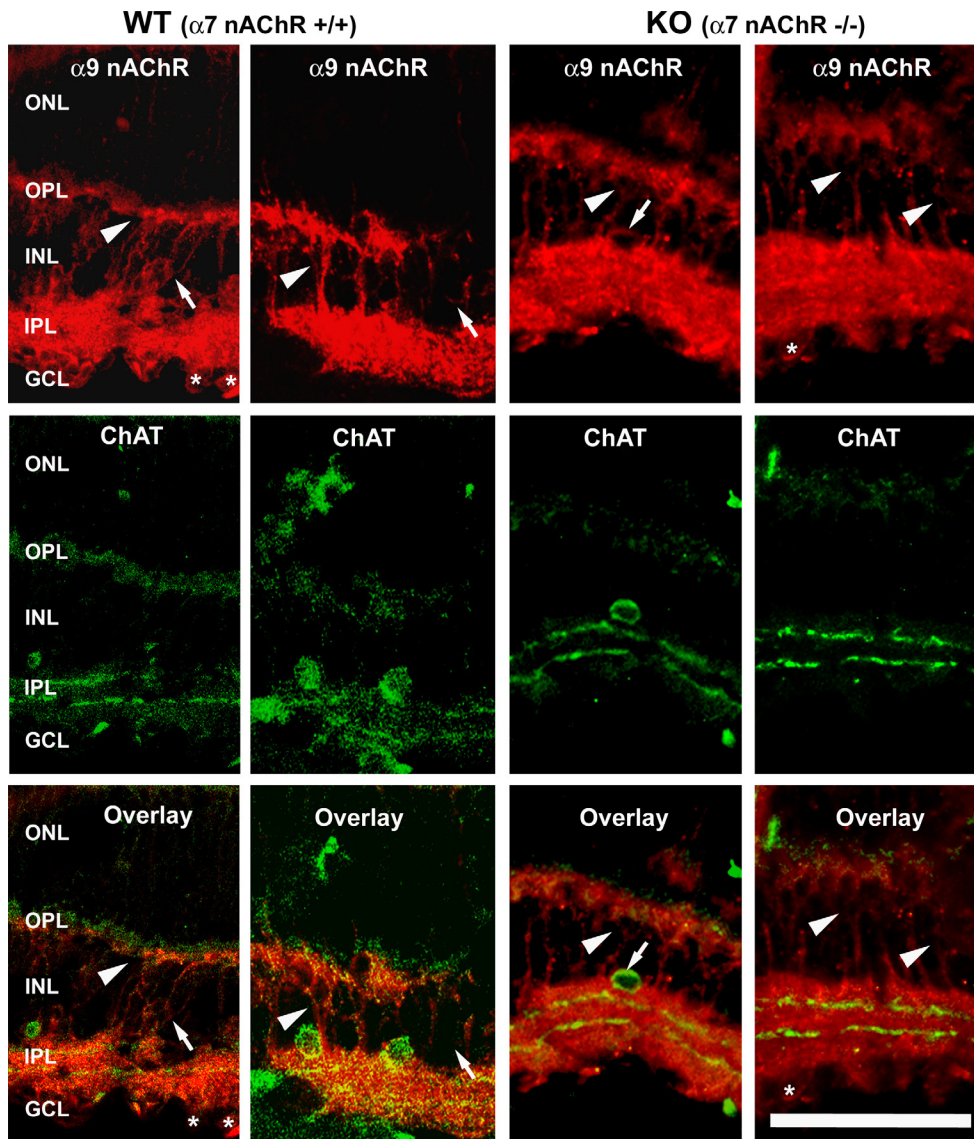
Figure 10. Labeling patterns of the α9 nAChR antibody (red) revealed labeling in the amacrine (arrows), bipolar (arrowheads), and ganglion cells (asterisks) with less cellular labeling in the α7 nAChR KO mouse retinas (right panels) than in the WT mouse retinas (left panels). The α9 nAChR immunoreactivity was broadly distributed through the IPL and encompassed the ChAT (green) immunoreactive bands. A subset of cholinergic amacrine cells demonstrated α9 immunoreactivity in the KO mouse retina. There were areas of increased density at the margins and in the center of the IPL, particularly in the KO mouse retinas, at the same level as the dim area in the center of the α3 and α5 nAChR immunoreactivity. Strong labeling in the outer plexiform layer (OPL) was consistent with the labeling of bipolar cell dendrites.

the ChAT (green) immunoreactive bands. There were areas of higher density labeling at the margins and in the center of the IPL, particularly in α7 nAChR KO mouse retinas at the same level as the weaker mAb 210 dendritic immuno-reactivity observed in a thin band in sublamina 3. The α9 nAChR immunoreactive amacrine cells did not appear to be immunoreactive for ChAT in WT mouse retinas, but a subset of cholinergic amacrine cells demonstrated α9 immunoreactivity in the α7 nAChR KO mouse retina.

Additionally, there was immunoreactivity at the level of the OPL, and many processes could be traced to the IPL or the OPL. These data are not completely consistent with the mRNA results indicating the upregulation of α9 nAChR transcripts in the whole retina, the oINL, and the GCL. The

mRNA upregulation only reached significance when qPCR was performed with the whole retina RNA. The oINL and the GCL mRNA alone were not significantly upregulated, which could lead to visual confirmation of these changes via IHC. Thus, a lack of qualitative differences in IHC does not rule out an increase in the overall α9 nAChR subunit proteins.

mAChR/ChAT double label IHC: Experiments using anti-bodies against mAChR subtypes showed differential immu-noreactivity between WT and α7 nAChR KO mouse retinas. Immunoreactivity in WT mouse retinas was limited to the ganglion cells, while immunoreactivity in α7 nAChR KO was evident in the amacrine cells, the bipolar cells, and throughout the IPL (Figure 11). Antibodies against m1 mAChRs labeled neurons throughout the GCL and two narrow bands of
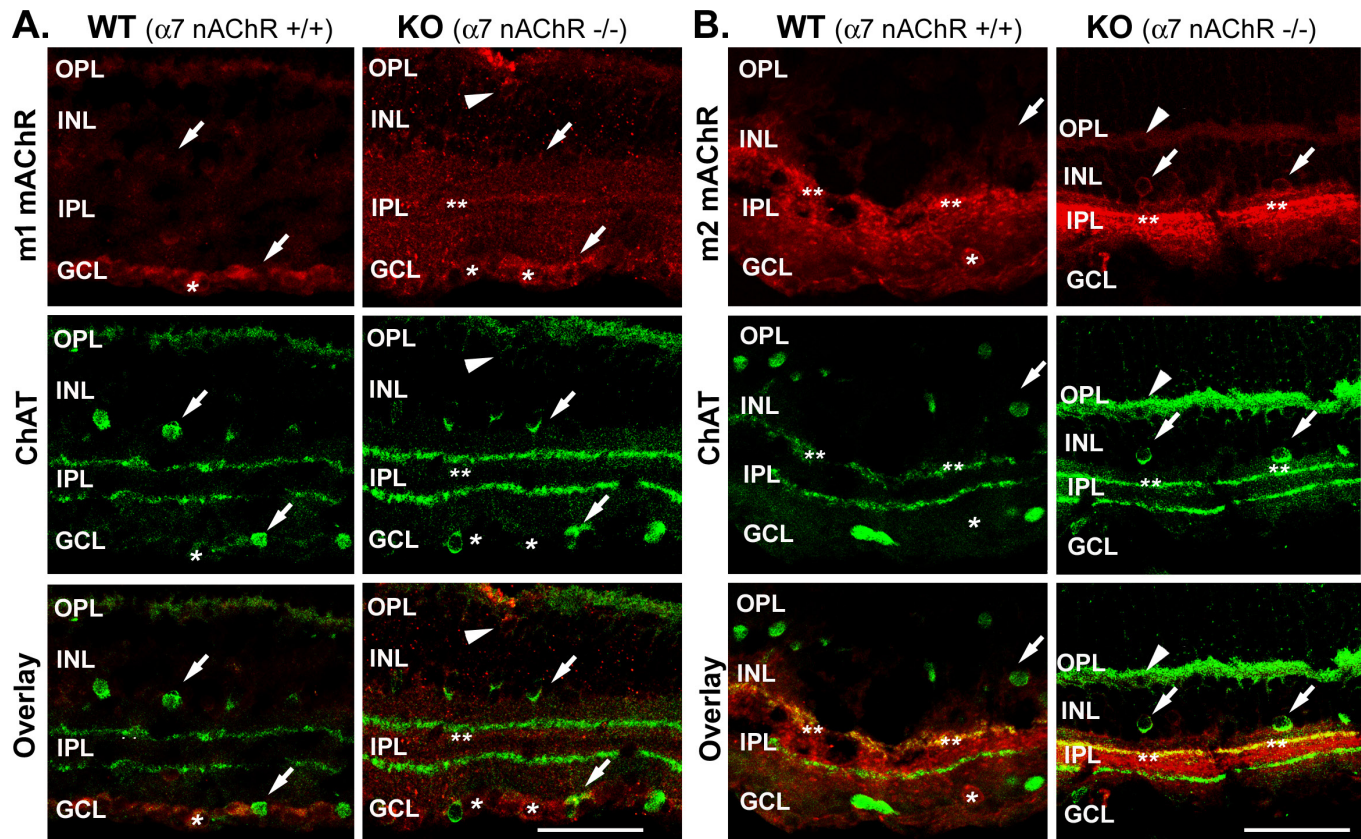
Figure 11. mAChR ICH in α7 nAChR KO and WT mouse retinas. (**A**) Labeling patterns of the m1 mAChR antibody (red) revealed labeling in ganglion cells (asterisks) in the WT and the α7 nAChR KO mouse retinas. There was broad diffuse IPL labeling in the IPL of the α7 nAChR KO mouse retinas as well as two bands of immunoreactivity (double asterisks) that were not evident in the IPL of the WT mouse retinas. The α9 immunoreactive IPL bands were directly beneath but did not colocalize with the ChAT (green) immunoreactive bands. (**B**) Labeling patterns of the m2 mAChR antibody (red) revealed labeling in the ganglion cells (asterisks) and labeling throughout the IPL of the WT mouse retinas. IPL labeling was more intense in in sublaminae 2 and 3 and colocalized with ChAT immunoreactivity in sublamina 2. There were no labeled cell bodies in the INL of the WT mouse retinas. In contrast, both bipolar (arrowheads) and amacrine cells, including cholinergic amacrine cells (arrows), were immunoreactive for m2 in the α7 nAChR KO mouse retinas. The brighter bands (double asterisks) within the IPL at sublaminae 2 and 3 were more intense in the α7 nAChR KO mouse retinas, and the colocalization with the ChAT (green) immunoreactive bands in sublamina 2 was more pronounced.

processes at sublamina 2 and sublamina 4, as well as diffuse labeling throughout the IPL in the α7 nAChR KO mouse retinas. The narrow bands of more intense immunoreactivity seen in the IPL of the α7 nAChR KO mouse retinas did not overlap with the ChAT immunoreactive bands, which are found at sublamina 2 and sublamina 4. The increased m1 mAChR immunoreactivity observed in the α7 nAChR KO mouse retina is consistent with the mRNA results, which showed an upregulation of m1 mAChRs in the α7 nAChR KO mouse retina.

Antibodies against m2 mAChRs in WT mouse retinas labeled ganglion cells and were distributed throughout the IPL with an increased density in sublaminae 2 and 3 that overlapped with ChAT immunoreactivity in sublamina 2. There were no m2-immunoreactive cells evident in the INL of

the WT mouse retinas. In contrast, both bipolar (arrowheads) and amacrine cells, including cholinergic amacrine cells (arrows), were immunoreactive for m2 in the α7 nAChR KO mouse retinas. IPL immunoreactivity was more pronounced in α7 nAChR KO mouse retinas, including immunoreactivity in sublamina 1 and increased density of the immunoreactivity in sublaminae 2 and 3. The mRNA results indicated significant an upregulation of the m2 transcripts within the GCL, suggesting that increased IPL labeling is mostly comprised of increased expressions of m2 AChRs by ganglion cells. The omission of primary antibodies resulted in no labeling, while the concentration-matched IgG controls displayed weak, non-specific labeling that did not resemble the experimental immunoreactivity patterns.

DISCUSSION

We wanted to understand why the elimination of a receptor subunit that is implicated in the development of the nervous system and that plays a role in normal vision resulted in a phenotype without significant observable phenotypic dysfunction. To assess the hypothesis that other AChR subunits and subtypes were upregulated to compensate for the loss of α7 nAChR subunits, we performed a series of qPCR, IHC, and western blotting experiments.

qPCR array screening: In this study, we assessed the abundance of AChR transcripts in α7 nAChR KO mouse retinas compared with WT mouse retinas to determine whether there were significant changes in the expressions of other AChR genes that are associated with the loss of the α7 nAChR subunit. The qPCR array results indicated a significant upregulation of the β2 GABA$_A$ receptor subunit and a significant downregulation of the Kcnj4 channel. The Kcnj4 channel is an inwardly-rectifying K$^+$ channel, responsible for helping return the cell membrane back to a resting potential [58]. The β2 GABA$_A$ receptor subunit is in the same super-family as nAChRs, and activation usually results in hyperpolarization [59]. Thus, a decrease in the Kcnj4 channel and an increase in the β2 GABA$_A$ receptor subunit may result in an increase in hyperpolarization. These results are counterintuitive; we speculated that a decrease in α7 nAChR-mediated excitation might correlate with a decrease in the inhibitory activity of β2 GABA$_A$ receptor subunits or an increase in Kcnj4, a channel that reduces the length of time a cell is hyperpolarized [60,61]. However, α7 nAChR activation can cause changes in the Ca^{2+}-dependent Cl$^-$ channel activity, and a decrease in the α7 nAChR-mediated activity could be linked to the observed decrease in Kcnj4 and the increase in β2 GABA$_A$ receptor subunits [62,63].

The qPCR array results also indicated a significant downregulation of the α5 nAChR subunit and the m1 mAChR subtype mRNA in the α7 nAChR KO mice. The α5 nAChR result was confirmed with qPCR using custom-designed AChR primers, but we did not detect a reduction in the m1 mAChR transcripts. In fact, the qPCR results using custom-designed and validated primers specific for the m1 mAChR subtype showed a significant upregulation. The differences in the expressions of the m1 mAChR subtype in the whole retina found by qPCR array and custom-designed primers could be due to the differences in the expressions across the retina, as seen in LCM qPCR results. This could reflect the unintentional loss of parts of the retina during retinal isolation, during which the GCL may be most vulnerable. However, due to the proprietary nature of the qPCR arrays, we did not have access to the validation and optimization data

for the m1 mAChR primers used and were unable to sequence the products to confirm that the m1 mAChR subtypes were in fact being amplified. Thus, the next set of experiments was performed with custom-designed and validated primers whose products could be sequenced.

α2, β2, β3, and β4 nAChR subunit qPCR: A comparison of the results of the different qPCR experiments helped to further parse differences in the AChR expressions in the α7 nAChR KO mouse retinas, as compared to the WT mouse retinas. Although, the whole retina qPCR results indicated a significant upregulation of the α2 nAChR subunit transcripts, a significant downregulation of the α2 nAChR subunits in the cells of the GCL, and a statistically non-significant downregulation in the INL. The upregulation in the whole retina, but not in the GCL and the INL, suggests that changes in the α2 nAChR subunit expressions occur in other areas of the retina, possibly within the endothelial cells of the retinal vasculature, as observed at the level of the OPL, or in the retinal macroglial cells, whose somas are in the OPL [6,64]. Both retinal vasculature and retinal macroglial cells have been shown to express nAChR subunits [6,64,65]. The neural retina was dissected from the retinal pigment epithelium (RPE) as carefully as possible before RNA extraction, but there could have been a contamination, and the observed upregulation might be attributable to RPE cells. The same changes observed in the α2 nAChR subunit transcripts in the KO mice were also observed in the β3 nAChR subunit transcripts; there was an overall upregulation but a significant downregulation in the oINL, the iINL, and the GCL. This implies that both the α2 and β3 nAChR subunits are increased in populations of cells other than retinal neurons, such as vascular endothelial cells or macrophages.

The patterns of changes in the abundance of β2 and β4 nAChR subunit transcripts were similar in the α7 nAChR KO mouse retinas compared with the WT mouse retinas; there was an overall upregulation in the whole retina, an upregulation in the oINL, and a downregulation in the GCL and in the iINL. This suggests that the β2- and β4-containing nAChRs were likely decreased in ganglion and amacrine cells and, perhaps, increased in bipolar cells and horizontal cells.

α5 nAChR subunit qPCR: Whole retina qPCR, using both SuperArray and custom primers, showed a significant downregulation of α3/α5 nAChR subunit transcripts, but the downregulation in the individual layers of the retina was not statistically significant. Additionally, IHC showed a reduction of α3/α5 nAChR subunit labeling intensity throughout the α7 nAChR KO mouse retinas, compared to the WT mouse retinas. This suggests that the overall downregulation of the α5 nAChR subunit involved several cell types and was not

specific to particular cell types of the retina, and the combined effect rises to significance. The α5 nAChR subunit is usually found in conjunction with the α3β4 subunits [66,67], and the downregulation of the α5 nAChR transcripts is consistent with a possible decrease in receptors with α3α5β4 stoichiometry. This suggests a shift in the ratio of α3α5β4 to α3β4 nAChRs in the retinas of the α7 nAChR KO mice. The α5-containing nAChRs are less sensitive to ACh and nicotine than other nAChRs, so a decrease in the abundance of these receptors might indicate an overall increase in sensitivity to ACh and nicotine [65].

α9 and α10 nAChR subunit qPCR: This study is the first to report α9 and α10 subunit expressions in mammalian retina. Because α9 and α10 nAChRs share several characteristics with α7 nAChRs, including high calcium permeability, we speculated that α9 and α10 subunits might be upregulated to compensate for the loss of the α7 subunits in the KO mouse retinas. Consistent with that prediction, α9 subunit transcripts were significantly upregulated when the expression was examined using mRNA extracted from the whole retina. However, there was also a significant downregulation of the α9 subunit in the iINL. This iINL downregulation suggests a reduction of the α9 subunit expression by populations of amacrine cells in the iINL. Consistent with this suggestion, there appeared to be fewer α9 subunit immunoreactive amacrine cells in the α7 nAChR KO mouse retinas than in the WT mouse retinas. While the α9 nAChR is typically assembled into an α9/10 heteromer, there have also been reports of α9 nAChR homomeric expressions in vitro [39,68]. The overall increase in the α9α10 transcripts in the α7 nAChR KO mouse retinas is consistent with the possibility that there is an increase in the α9 nAChR and α9α10 nAChRs when compared to WT mouse retinas. These increases were likely limited to the GCL, since both α9 subunit and α10 subunit transcripts were reduced in the RNA extracted from the total INL cells gathered by LCM.

m1, m2, and m4 mAChR subtype qPCR: The m1 mAChR subtype showed a significant upregulation in the whole retina, and it trended toward upregulation in the oINL and the GCL and downregulation in the iINL. The upregulation in the oINL and GCL together was not sufficient to reach significance, but when the whole retina was examined, the upregulation was significant. There were also cell-type specific changes detected in both m2 and m4 mAChR subtypes. While the m2 mAChR subtype showed no significant changes in expression in the whole retina, there was a significant upregulation in the GCL and a significant downregulation in the iINL. These changes suggest the possibility of an increased inhibition via the m2 mAChR subtype in the

cells of the GCL and a decrease in the inhibition of amacrine cells in the iINL.

Western blot and IHC: To confirm the presence of AChR protein and confirm the specificity of antibodies used in IHC experiments, a series of western blot experiments were completed. Protein expression and antibody specificity were confirmed for α3, α5, and α9 nAChR subunits as well as m1, m2, and m4 mAChR subtypes.

While α5 nAChR subunit protein expression patterns have not been previously examined in mouse retina, the expression patterns obtained were similar to those observed in rabbit retina, with the addition of the expression by the bipolar cells. Specifically, mouse retina amacrine, bipolar, and ganglion cells displayed immunoreactivity for α3 and α5 nAChR subunits, and immunoreactivity was detectable throughout the IPL. In rabbit retina, the patterns are identical, except that in the rabbit retina, the bipolar cells that display α3 and α5 nAChR subunit immunoreactivity are absent [4]. A population of ON cone bipolar cells has been shown to express α7 nAChR subunits [5]. These nAChRs respond to high concentrations of ACh and nicotine transiently with fast desensitization, while the responses of non-α7 nAChRs, such as those containing α3 or α5 nAChR subunits, have less rapid desensitization [69,70]. We speculate that the α3 and α5 nAChR subunit containing bipolar cells in the mouse retina have a more sustained response than the α7 nAChR subunit containing bipolar cells in the rabbit retina. A more sustained bipolar response may result in enhanced glutamate released from the cholinoceptive bipolar cells in the mouse retina.

An immunoprecipation study by Origlia [47] indicated no significant differences in the protein levels of α2, α5, and β4 nAChR subunits in the α7 nAChR KO mouse retina. However, the Origlia study used whole retina protein extracts and did not examine protein expressions in different retinal cell populations. As we observed in our LCM qPCR experiments, variations in the expressions within specific cell populations would be undetectable in studies using whole retina extracts.

AB49065, a commercially available antibody that recognizes α9 nAChR subunits, revealed immunoreactivity in presumptive bipolar, amacrine, and ganglion cells in the retina. Additionally, AB49065 immunoreactivity was detected in the IPL and was most intense in sublamina 3. The specificity of AB49065 was confirmed with western blot, and protein extracted from a α9 nAChR KO mouse retina was used. Incubation with AB49065 did not result in labeling on western blots, further confirming antibody specificity.

In general, nAChRs are activated by ACh and nicotine but blocked by curare, while mAChRs are activated by ACh and muscarine but blocked by atropine. The nAChRs allow all cations to move through the channels with varying levels of permeability, but the α7 nAChRs have the highest Ca^{2+} permeability of all the nAChRs [71]. Additionally, α7 nAChRs are blocked by low micromolar concentrations of strychnine, as well as by α-bungarotoxin [72].

However, experiments that rely on nicotine to activate nAChRs would not detect α9 nAChRs because they have a different pharmacological profile than the other nAChRs. They are activated by ACh, carbachol, and choline, but not by nicotine. They are blocked by α-BGT, strychnine, and atropine and have high Ca^{2+} permeability [28-36]. To our knowledge, this is the first report of α9-containing AChRs in the retina. The pharmacology of these receptors is complex. This complexity makes it difficult to detect α9 AChRs with pharmacological tools.

In addition, m1 mAChR subtype immunoreactivity in the IPL was more intense and distinct in the α7 nAChR KO mouse retinas than in the WT mouse retinas, which is consistent with the qPCR data. The results of qPCR and IHC studies suggest the possibility of increased excitation via m1 mAChR subunits in the oINL and GCL and decreased excitation in the iINL. However, amacrine cells in the iINL release GABA or glycine, thus, decreased excitation of the amacrine cells would actually result in an overall decrease in the amacrine-cell-induced inhibition of other cell types.

There was also increased m2 mAChR immunoreactivity in the iINL and the IPL of the α7 nAChR KO mouse retinas. Increased m2 transcripts in the GCL of α7 nAChR KO mouse retinas suggest that the IPL increases were due to increased expressions of m2 AChRs by ganglion cells, and they provided a pathway for the cholinergic inhibition of ganglion cell responses. The colocalization of m2 and ChAT in both WT and α7 nAChR KO mouse retinas suggests that m2 mAChRs provide autofeedback to the OFF population of cholinergic amacrine cells.

The m4 mAChR subtype was significantly upregulated in the whole retina as well as in the oINL and the GCL, and it was significantly downregulated in the iINL. This suggests that there may also be an increase in direct inhibition via m4 mAChRs on cells in the oINL and the GCL and a decrease in indirect inhibition mediated by GABAergic or glycinergic cells in the iINL.

ChAT wholemount IHC: The qPCR screening studies did not show any differences in the ChAT expressions in the α7 nAChR KO mouse retinas, but to further assess the possibility of any alterations in the distribution or number of ChAT immunoreactive cells in the retina, we performed cell counts. Consistent with previous reports in rabbits, mice, and other mammals, ChAT immunoreactivity was observed in amacrine cell bodies in the INL, amacrine cell bodies in the GCL, and two distinct bands of labeling in the IPL [56,57]. Also consistent with previous reports, there was a significantly higher number of ChAT-positive amacrine cells in the INL compared to the GCL. However, there were no significant differences in the number of cholinergic cells in the WT mouse retinas compared to the α7 nAChR KO mouse retinas.

Implications: The findings of the current study demonstrate that the absence of α7 nAChRs does not simply correlate with changes in the mRNA expressions of other AChR subunits or subtypes. Instead, there is a complex pattern of changes in the expressions of different nAChR subunits and mAChR subtypes, with variations across retinal cell populations. Additionally, our results may suggest changes in the number of receptor subtypes, resulting in differing affinities for ACh and choline, as well as an overall decrease in amacrine cell-mediated inhibition, which could, in part, compensate for the loss of the excitatory α7 nAChRs.

REFERENCES

1. Famiglietti EV. On and off pathways through amacrine cells in mammalian retina: the synaptic connections of "starburst" amacrine cells. Vision Res 1983; 23:1265-79. [PMID: 6362185].

2. Masland RH, Mills JW, Cassidy C. The functions of acetylcholine in the rabbit retina. Proc R Soc Lond B Biol Sci 1984; 223:121-39. [PMID: 6151181].

3. Famiglietti EV. 'Starburst' amacrine cells and cholinergic neurons: mirror-symmetric on and off amacrine cells of rabbit retina. Brain Res 1983; 261:138-44. [PMID: 6301622].

4. Keyser KT, MacNeil MA, Dmitrieva N, Wang F, Masland RH, Lindstrom JM. Amacrine, ganglion and displaced amacrine cells in the rabbit retina express nicotinic acetylcholine receptors. Vis Neurosci 2000; 17:743-52. [PMID: 11153654].

5. Dmitrieva NA, Strang CE, Keyser KT. Expression of alpha 7 nicotinic acetylcholine receptors by bipolar, amacrine, and

ganglion cells of the rabbit retina. J Histochemistry Society. 2007; 55:461-76. [PMID: 17189521].

6. Liu J, McGlinn AM, Fernandes A, Milam AH, Strang CE, Andison ME, Lindstrom JM, Keyser KT, Stone RA. Nicotinic acetylcholine receptor subunits in rhesus monkey retina. Invest Ophthalmol Vis Sci 2009; 50:1408-15. [PMID: 18952912].

7. Strang CE, Renna JM, Amthor FR, Keyser KT. Muscarinic acetylcholine receptor localization and activation effects on ganglion response properties. Invest Ophthalmol Vis Sci 2010; 51:2778-89. [PMID: 20042645].

8. Blute TA, Strang C, Keyser KT, Eldred WD. Activation of the cGMP/nitric oxide signal transduction system by nicotine in the retina. Vis Neurosci 2003; 20:165-76. [PMID: 12916738].

9. Cimini BA, Strang CE, Wotring VE, Keyser KT, Eldred WD. Role of acetylcholine in nitric oxide production in the salamander retina. J Comp Neurol 2008; 507:1952-63. [PMID: 18273886].

10. Baldridge WH. Optical recordings of the effects of cholinergic ligands on neurons in the ganglion cell layer of mammalian retina. J Neurosci 1996; 16:5060-72. [PMID: 8756436].

11. Kittila CA, Massey SC. Pharmacology of directionally selective ganglion cells in the rabbit retina. J Neurophysiol 1997; 77:675-89. [PMID: 9065840].

12. Zhou ZJ, Zhao D. Coordinated transitions in neurotransmitter systems for the initiation and propagation of spontaneous retinal waves. J Neurosci 2000; 20:6570-7. [PMID: 10964962].

13. Brown DA, Abogadie FC, Allen TG, Buckley NJ, Caulfield MP, Delmas P, Haley JE, Lamas JA, Selyanko AA. Muscarinic mechanisms in nerve cells. Life Sci 1997; 60:1137-44. [PMID: 9121358].

14. Caulfield MP, Birdsall NJ. International Union of Pharmacology. XVII. Classification of muscarinic acetylcholine receptors. Pharmacol Rev 1998; 50:279-90. [PMID: 9647869].

15. Wess J, Liu J, Blin N, Yun J, Lerche C, Kostenis E. Structural basis of receptor/G protein coupling selectivity studied with muscarinic receptors as model systems. Life Sci 1997; 60:1007-14. [PMID: 9121341].

16. Karlin A. Emerging structure of the nicotinic acetylcholine receptors. Nat Rev Neurosci 2002; 3:102-14. [PMID: 11836518].

17. Alexander SP, Mathie A, Peters JA. Guide to Receptors and Channels (GRAC), 2nd edition (2007 Revision). Br J Pharmacol. 2007 Feb;150 Suppl 1:S1–168.

18. Simard AR, Gan Y, St-Pierre S, Kousari A, Patel V, Whiteaker P, Morley BJ, Lukas RJ, Shi FD. Differential modulation of EAE by alpha9*- and beta2*-nicotinic acetylcholine receptors. Immunol Cell Biol 2013; 91:195-200. [PMID: 23399696].

19. Morley BJ, Li HS, Hiel H, Drescher DG, Elgoyhen AB. Identification of the subunits of the nicotinic cholinergic receptors in the rat cochlea using RT-PCR and in situ hybridization. Brain Res Mol Brain Res 1998; 53:78-87. [PMID: 9473597].

20. Morley BJ, Simmons DD. Developmental mRNA expression of the alpha10 nicotinic acetylcholine receptor subunit in the rat cochlea. Brain Res Dev Brain Res 2002; 139:87-96. [PMID: 12414097].

21. Clementi F, Fornasari D, Gotti C. Neuronal nicotinic acetylcholine receptors: from structure to therapeutics. Trends Pharmacol Sci 2000; 21:35-7. [PMID: 10733431].

22. Lindstrom JM. The structures of neuronal nicotinic receptors. In: Clementi F, Fornasari D, Gotti C, editors. Handbook of Experimental Pharmacology Vol 144. Berlin Heidelburg: Springer-Verlag; 2000. p. 101–62.

23. McGehee DS. Molecular diversity of neuronal nicotinic acetylcholine receptors. Ann N Y Acad Sci 1999; 868:565-77. [PMID: 10414338].

24. Lindstrom J, Anand R, Gerzanich V, Peng X, Wang F, Wells G. Structure and function of neuronal nicotinic acetylcholine receptors. Prog Brain Res 1996; 109:125-37. [PMID: 9009699].

25. Lindstrom JM. Neuronal nicotinic acetylcholine receptors. In: Narahashi T, editor. Ion Channels, Volume 4. New York: Plenum Press; 1996. p. 377–449.

26. Arias HR. Localization of agonist and competitive antagonist binding sites on nicotinic acetylcholine receptors. Neurochem Int 2000; 36:595-645. [PMID: 10771117].

27. Khiroug SS, Harkness PC, Lamb PW, Sudweeks SN, Khiroug L, Millar NS, Yakel JL. Rat nicotinic ACh receptor alpha7 and beta2 subunits co-assemble to form functional heteromeric nicotinic receptor channels. J Physiol 2002; 540:425-34. [PMID: 11956333].

28. Housley GD, Ashmore JF. Direct measurement of the action of acetylcholine on isolated outer hair cells of the guinea pig cochlea. Proc Biol Sci 1991; 244:161-7. [PMID: 1679550].

29. Fuchs PA, Murrow BW. A novel cholinergic receptor mediates inhibition of chick cochlear hair cells. Proc Biol Sci 1992; 248:35-40. [PMID: 1355909].

30. Elgoyhen AB, Johnson DS, Boulter J, Vetter DE, Heinemann S. Alpha 9: an acetylcholine receptor with novel pharmacological properties expressed in rat cochlear hair cells. Cell 1994; 79:705-15. [PMID: 7954834].

31. Erostegui C, Norris CH, Bobbin RP. In vitro pharmacologic characterization of a cholinergic receptor on outer hair cells. Hear Res 1994; 74:135-47. [PMID: 8040084].

32. Johnson DS, Martinez J, Elgoyhen AB, Heinemann SF, McIntosh JM. alpha-Conotoxin ImI exhibits subtype-specific nicotinic acetylcholine receptor blockade: preferential inhibition of homomeric alpha 7 and alpha 9 receptors. Mol Pharmacol 1995; 48:194-9. [PMID: 7651351].

33. Dulon D, Lenoir M. Cholinergic responses in developing outer hair cells of the rat cochlea. Eur J Neurosci 1996; 8:1945-52. [PMID: 8921285].

34. Evans MG. Acetylcholine activates two currents in guinea-pig outer hair cells. J Physiol 1996; 491:563-78. [PMID: 8866879].

35. Rothlin CV, Katz E, Verbitsky M, Elgoyhen AB. The alpha9 nicotinic acetylcholine receptor shares pharmacological properties with type A gamma-aminobutyric acid, glycine, and type 3 serotonin receptors. Mol Pharmacol 1999; 55:248-54. [PMID: 9927615].

36. Katz E, Verbitsky M, Rothlin CV, Vetter DE, Heinemann SF, Elgoyhen AB. High calcium permeability and calcium block of the alpha9 nicotinic acetylcholine receptor. Hear Res 2000; 141:117-28. [PMID: 10713500].

37. Elgoyhen AB, Vetter DE, Katz E, Rothlin CV, Heinemann SF, Boulter J. alpha10: a determinant of nicotinic cholinergic receptor function in mammalian vestibular and cochlear mechanosensory hair cells. Proc Natl Acad Sci USA 2001; 98:3501-6. [PMID: 11248107].

38. Gerzanich V, Wang F, Kuryatov A, Lindstrom J. alpha 5 Subunit alters desensitization, pharmacology, Ca++ permeability and Ca++ modulation of human neuronal alpha 3 nicotinic receptors. J Pharmacol Exp Ther 1998; 286:311-20. [PMID: 9655874].

39. Weisstaub N, Vetter DE, Elgoyhen AB, Katz E. The alpha9alpha10 nicotinic acetylcholine receptor is permeable to and is modulated by divalent cations. Hear Res 2002; 167:122-35. [PMID: 12117536].

40. Alkondon M, Albuquerque EX. Nicotinic acetylcholine receptor alpha7 and alpha4beta2 subtypes differentially control GABAergic input to CA1 neurons in rat hippocampus. J Neurophysiol 2001; 86:3043-55. [PMID: 11731559].

41. Strang CE, Renna JM, Amthor FR, Keyser KT. Nicotinic acetylcholine receptor expression by directionally selective ganglion cells. Vis Neurosci 2007; 24:523-33. [PMID: 17686198].

42. Coyle JT, Price DL, DeLong MR. Alzheimer's disease: a disorder of cortical cholinergic innervation. Science 1983; 219:1184-90. [PMID: 6338589].

43. Nordberg A. PET studies and cholinergic therapy in Alzheimer's disease. Rev Neurol (Paris) 1999; 155:Suppl 4S53-63. [PMID: 10637939].

44. Leonard S, Freedman R. Genetics of chromosome 15q13-q14 in schizophrenia. Biol Psychiatry 2006; 60:115-22. [PMID: 16843094].

45. Xu J, Pato MT, Torre CD, Medeiros H, Carvalho C, Basile VS, Bauer A, Dourado A, Valente J, Soares MJ, Macedo AA, Coelho I, Ferreira CP, Azevedo MH, Macciardi F, Kennedy JL, Pato CN. Evidence for linkage disequilibrium between the alpha 7-nicotinic receptor gene (CHRNA7) locus and schizophrenia in Azorean families. Am J Med Genet 2001; 105:669-74. [PMID: 11803513].

46. Morley BJ, Rodriguez-Sierra JF. A phenotype for the alpha 7 nicotinic acetylcholine receptor null mutant. Brain Res 2004; 1023:41-7. [PMID: 15364017].

47. Origlia N, Valenzano DR, Moretti M, Gotti C, Domenici L. Visual acuity is reduced in alpha 7 nicotinic receptor knockout mice. Invest Ophthalmol Vis Sci 2012; 53:1211-8. [PMID: 22281823].

48. Paylor R, Nguyen M, Crawley JN, Patrick J, Beaudet A, Orr-Urtreger A. Alpha7 nicotinic receptor subunits are not necessary for hippocampal-dependent learning or sensorimotor gating: a behavioral characterization of Acra7-deficient mice. Learn Mem 1998; 5:302-16. [PMID: 10454356].

49. Young JW, Crawford N, Kelly JS, Kerr LE, Marston HM, Spratt C, Finlayson K, Sharkey J. Impaired attention is central to the cognitive deficits observed in alpha 7 deficient mice. Eur Neuropsychopharmacol 2007; 17:145-55. [PMID: 16650968].

50. Fernandes C, Hoyle E, Dempster E, Schalkwyk LC, Collier DA. Performance deficit of alpha7 nicotinic receptor knockout mice in a delayed matching-to-place task suggests a mild impairment of working/episodic-like memory. Genes Brain Behav 2006; 5:433-40. [PMID: 16923147].

51. Egea J, Rosa AO, Sobrado M, Gandia L, Lopez MG, Garcia AG. Neuroprotection afforded by nicotine against oxygen and glucose deprivation in hippocampal slices is lost in alpha7 nicotinic receptor knockout mice. Neuroscience 2007; 145:866-72. [PMID: 17291692].

52. Grabus SD, Martin BR, Batman AM, Tyndale RF, Sellers E, Damaj MI. Nicotine physical dependence and tolerance in the mouse following chronic oral administration. Psychopharmacology (Berl) 2005; 178:183-92. [PMID: 15365686].

53. Nolan T, Hands RE, Bustin SA. Quantification of mRNA using real-time RT-PCR. Nat Protoc 2006; 1:1559-82. [PMID: 17406449].

54. Gu YH, Zhang ZM, Long T, Li L, Hou BK, Guo Q. A naturally occurring rat model of X-linked cone dysfunction. Invest Ophthalmol Vis Sci 2003; 44:5321-6. [PMID: 14638733].

55. Herber DL, Severance EG, Cuevas J, Morgan D, Gordon MN. Biochemical and histochemical evidence of nonspecific binding of alpha7nAChR antibodies to mouse brain tissue. J Histochem Cytochem 2004; 52:1367-76. [PMID: 15385583].

56. Galli-Resta L, Novelli E, Volpini M, Strettoi E. The spatial organization of cholinergic mosaics in the adult mouse retina. Eur J Neurosci 2000; 12:3819-22. [PMID: 11029653].

57. Haverkamp S, Wassle H. Immunocytochemical analysis of the mouse retina. J Comp Neurol 2000; 424:1-23. [PMID: 10888735].

58. Kubo Y, Adelman JP, Clapham DE, Jan LY, Karschin A, Kurachi Y, Lazdunski M, Nichols CG, Seino S, Vandenberg CA. International Union of Pharmacology. LIV. Nomenclature and molecular relationships of inwardly rectifying potassium channels. Pharmacol Rev 2005; 57:509-26. [PMID: 16382105].

59. Hadingham KL, Wingrove PB, Wafford KA, Bain C, Kemp JA, Palmer KJ, Wilson AW, Wilcox AS, Sikela JM, Ragan CI, Whiting PJ. Role of the beta subunit in determining the pharmacology of human gamma-aminobutyric acid type

A receptors. Mol Pharmacol 1993; 44:1211-8. [PMID: 8264558].

60. Isomoto S, Kondo C, Kurachi Y. Inwardly rectifying potassium channels: their molecular heterogeneity and function. Jpn J Physiol 1997; 47:11-39. [PMID: 9159640].

61. Hibino H, Inanobe A, Furutani K, Murakami S, Findlay I, Kurachi Y. Inwardly rectifying potassium channels: their structure, function, and physiological roles. Physiol Rev 2010; 90:291-366. [PMID: 20086079].

62. Yamashita T, Isa T. Fulfenamic acid sensitive, Ca(2+)-dependent inward current induced by nicotinic acetylcholine receptors in dopamine neurons. Neurosci Res 2003; 46:463-73. [PMID: 12871768].

63. Zhang J, Berg DK. Reversible inhibition of GABAA receptors by alpha7-containing nicotinic receptors on the vertebrate postsynaptic neurons. J Physiol 2007; 579:753-63. [PMID: 17204496].

64. Arias HR, Richards VE, Ng D, Ghafoori ME, Le V, Mousa SA. Role of non-neuronal nicotinic acetylcholine receptors in angiogenesis. Int J Biochem Cell Biol 2009; 41:1441-51. [PMID: 19401144].

65. Jackson KJ, Marks MJ, Vann RE, Chen X, Gamage TF, Warner JA, Damaj MI. Role of alpha5 nicotinic acetylcholine receptors in pharmacological and behavioral effects of nicotine in mice. J Pharmacol Exp Ther 2010; 334:137-46. [PMID: 20400469].

66. Sargent PB. The diversity of neuronal nicotinic acetylcholine receptors. Annu Rev Neurosci 1993; 16:403-43. [PMID: 7681637].

67. Gotti C, Fornasari D, Clementi F. Human neuronal nicotinic receptors. Prog Neurobiol 1997; 53:199-237. [PMID: 9364611].

68. Plazas PV, Katz E, Gomez-Casati ME, Bouzat C, Elgoyhen AB. Stoichiometry of the alpha9alpha10 nicotinic cholinergic receptor. J Neurosci 2005; 25:10905-12. [PMID: 16306403].

69. Papke RL, Bencherif M, Lippiello P. An evaluation of neuronal nicotinic acetylcholine receptor activation by quaternary nitrogen compounds indicates that choline is selective for the alpha 7 subtype. Neurosci Lett 1996; 213:201-4. [PMID: 8873149].

70. Papke RL, Meyer E, Uteshev VV. α7 Receptor-selective agonists and modes of à7 receptor activation. Eur J Pharmacol 2000; 393:179-95. [PMID: 10771012].

71. Fucile S. Ca(2+) permeability of nicotinic acetylcholine receptors. Cell Calcium 2004; 35:1-8. [PMID: 14670366].

72. Renna JM, Strang CE, Amthor FR, Keyser KT. Strychnine, but not PMBA, inhibits neuronal nicotinic acetylcholine receptors expressed by rabbit retinal ganglion cells. Vis Neurosci 2007; 24:503-11. [PMID: 17900376].